AN ANALYSIS OF THE MARINER 4 PHOTOGRAPHY OF MARS

C. R. CHAPMAN, J. B. POLLACK, and C. SAGAN

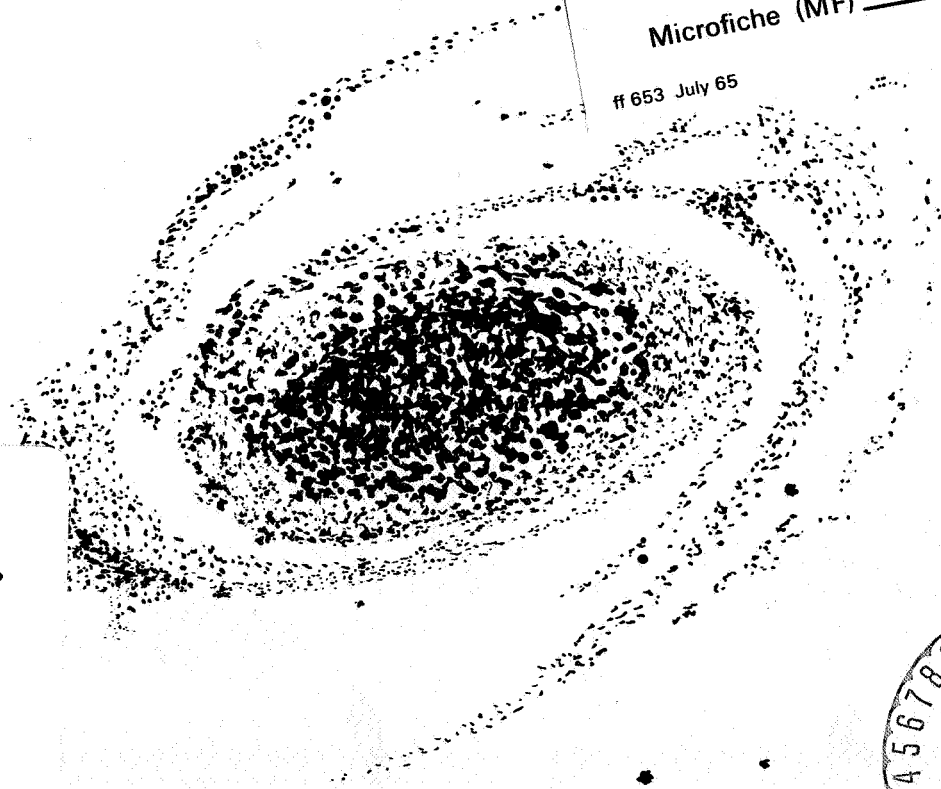

Smithsonian Astrophysical Observatory
SPECIAL REPORT 268

Research in Space Science
SAO Special Report No. 268

AN ANALYSIS OF THE MARINER 4 PHOTOGRAPHY OF MARS

Clark R. Chapman, James B. Pollack, and Carl Sagan

February 14, 1968

Smithsonian Institution
Astrophysical Observatory
Cambridge, Massachusetts 02138

708-11

TABLE OF CONTENTS

LIST OF ILLUSTRATIONS

LIST OF TABLES

ABSTRACT

A catalog of nearly 300 craters and crater-like objects has been prepared from several sets of contrast-enhanced high-quality positive transparencies of the Mariner 4 photography. Craters were identified and counted by the same procedures used in the compilation of lunar crater catalogs; particular attention was given to crater class and quality. Counts of craters with diameters $D < 20$ km begin to show the effects of incompleteness. A direct inspection of the photographs as well as the constancy of crater class proportions with crater diameter interval above 20 km indicates that substantial erosion and obliteration of all but the largest craters have occurred during the history of Mars. The epochs of crater formation and crater erosion appear to be closely tied together in time.

A statistical curve-fitting program for the observed crater diameter-frequency relations and a differential number-density distribution law of AD^{-B} give $B = 2.5 \pm 0.2$ for $D > 20$ km or $B = 3.0 \pm 0.2$ for $D > 30$ km. The population of impacting objects assumed responsible for these craters is taken as having a differential number density varying as $X^{-\beta}$, where X is the diameter of the impacting object. The number of "live" comets and Apollo objects crossing the orbit of Mars is insufficient by more than 2 orders of magnitude to explain the observed number density of craters on Mars. For asteroidal objects with $\beta = 2$ or 3, the predicted and observed number densities cannot be brought into agreement unless we assume an early epoch of very high cratering rates on Mars. For $\beta = 4$ or 5, agreement between the predicted and observed number densities can be secured with a nearly uniform rate of asteroidal bombardment. The absence of saturation bombardment of Mars for very large craters points to a value of β significantly above 3. This is not inconsistent with expectations for asteroids with $X > 1$ km in the inner part of the asteroid belt. In this case, crater diameter scales with kinetic energy, W, of the impacting object as $W^{1/3}$.

For all reasonable values of β, impact damage contributes to crater erosion and obliteration. The fraction of the surface covered by craters is of the order unity. For all reasonable values of β, asteroidal bombardment is capable of accounting quantitatively for the observed values of both A and B, particularly if the zone of obliteration around Martian craters is larger than that for lunar craters. For near-saturation bombardment, the existing observations are of very little use in determining the value of β, or in distinguishing between saturation bombardment and such other erosion mechanisms as windblown dust of impact or of micrometeoric origin; liquid water on macro or microscales; mountain building; and flooding by lava. The dust produced by impact during the history of Mars is estimated to have depths between 0.1 and several kilometers. The diameter of the largest crater obliterated in 4.5×10^9 years is calculated to be between 60 and 180 km; for the lifetime against erosion, assumed to scale as D^a, we calculate $a \simeq 0$ for $\beta = 2$ or 3, and $1 \leq a \leq 2.5$ for $\beta = 4$ or 5.

For $\beta < 3$, the mean ages of Martian craters are found to be approximately equal to the age of the planet. However, for β significantly larger than 3, different craters will have different mean ages, ranging from about 2.25×10^9 years for the very largest craters, down to some tens of millions of years or less for craters smaller than 20 km. In this case, surface features of the order of 10 km in width or smaller may have been quite prominent in the early history of Mars and undetectable on the Mariner 4 photographs. Thus, the absence of such signs of running water as river valleys in the Mariner 4 photography is quite irrelevant to the question of the existence of bodies of water in early Martian history. These conclusions on ages are independent of estimates of the ages of lunar maria. Some weak evidence exists for a correlation between high crater density and dark areas on Mars.

RÉSUMÉ

Un catalogue de près de 300 cratères et objets en forme de cratère a été préparé à partir de plusieurs jeux de copies diapositives de très bonne qualité et à contrastes accentués, de la photographie originale prise par Mariner 4. Les cratères furent identifiés et comptés en employant les mêmes méthodes que celles utilisées dans la préparation des catalogues des cratères lunaires; une attention particulière a été accordée à la classe et à la qualité des cratères. Le dénombrement des cratères de diamètre $D < 20$ km commence à montrer les évidences d'un caractère incomplet. L'observation directe des photographies ainsi que le fait que la répartition en classes des cratères ne varie pas avec l'intervalle de diamètre considéré, pour des diamètres supérieurs à 20 km, indiquent que tous les cratères à part les plus grands ont été soumis à une érosion et à une destruction importantes au cours de l'histoire de Mars. Les époques de formation et d'érosion des cratères sont étroitement reliées dans le temps.

En remplaçant la distribution observée des cratères en fonction de leur diamètre par une courbe continue obtenue par méthode statistique et en supposant une densité différentielle du nombre des cratères, de la forme AD^{-B}, on obtient $B = 2,5 \pm 0,2$ pour $D > 20$ km, ou $B = 3,0 \pm 0,2$ pour $D > 30$ km. On suppose ensuite que la population des projectiles considérés comme responsables de la formation des cratères, est telle que la densité différentielle du nombre des projectiles varie comme $X^{-\beta}$ en fonction du diamètre X du projectile. Le nombre des comètes "actives" et d'objets du type "Apollo" qui traversent l'orbite de Mars, est trop faible par plus de deux ordres de grandeur pour pouvoir rendre compte de la densité du nombre des cratères observés sur Mars. Dans le cas d'objets du type astéroïde pour lesquels $\beta = 2$ ou 3, les densités calculées et observées ne sont en bon accord que si l'on suppose une époque initiale caractérisée par un très fort taux de formation des cratères sur Mars. Pour $\beta = 4$ ou 5, l'accord entre les densités observées et

calculées peut être assuré moyennant un taux de bombardement astéroïdal presque uniforme. L'absence de bombardement de saturation pour les plus grands cratères semble indiquer une valeur de β supérieure à 3 de façon appréciable. Cette hypothèse n'est pas en contradiction avec les estimations faites pour les astéroïdes de diamètre supérieur à 1 km dans la partie inférieure de la ceinture astéroïdale. Dans ce cas le diamètre du cratère varie avec l'énergie cinétique W du projectile comme $W^{1/3}$.

Pour toutes valeurs raisonnables de β, les dommages à l'impact contribuent à l'érosion et à la destruction du cratère. La proportion de surface couverte par les cratères est de l'ordre unité. Pour toutes valeurs raisonnables de β, le bombardement astéroïdal est capable de rendre compte quantitativement des valeurs observées pour A, aussi bien que pour B, surtout si la zone de destruction autour des cratères est plus grande dans le cas de Mars que dans le cas des cratères lunaires. Pour des bombardements proches de la saturation, les observations obtenues sont d'une utilité très réduite pour déterminer la valeur de β ou pour distinguer entre le bombardement de saturation et d'autres sources d'érosion telles que la poussière d'impact soufflée par le vent ou d'origine micrométéoritique, l'eau liquide en grande quantité ou à l'échelle microscopique, la formation de montagnes et les écoulements de lave. La couche de poussière produite par impact au cours de l'histoire de Mars a été estimée d'une profondeur de 0,1 à plusieurs kilomètres. Les calculs ont montré que le plus grand cratère détruit en $4,5 \times 10^9$ années a un diamètre entre 60 et 180 km; pour la durée de survie à l'érosion, que l'on suppose de la forme D^{α}, α a été trouvé voisin de zéro pour $\beta = 2$ ou 3, et $1 \leq \alpha \leq 2,5$ pour $\beta = 4$ ou 5.

Pour $\beta < 3$, les âges moyens des cratères sur Mars ont été trouvés approximativement égaux à l'âge de la planète. Toutefois, pour $\beta > 3$ de manière appréciable, des cratères différents auront des âges moyens différents, allant d'environ $2,25 \times 10^9$ années pour les plus grands jusqu'à quelques dizaines de millions d'années ou moins pour les cratères de diamètre inférieur à 20 km. Auquel cas il est possible que des reliefs de surface de l'ordre de 10 km de largeur ou moins aient pu être

très marqués au début de l'histoire de Mars sans que l'on puisse les déceler sur les photographies de Mariner 4. Ainsi, l'absence de signes indiquant la présence d'eau courante tels que des vallées de fleuve, sur la photographie de Mariner 4 ne fournit aucune information quant à la présence de nappes d'eau au début de l'histoire de Mars. Ces conclusions concernant les âges sont indépendantes des âges estimés des mers lunaires. Il existe une faible indication d'une corrélation entre les zones à forte densité de cratères et les zones sombres de Mars.

КОНСПЕКТ

Каталог примерно 300 кратеров и подобных кратеру предметов был приготовлен исходя из нескольких серий сильно контрастных, высококачественных позитивных транспарантов фотоснимков сделанных Маринером 4. Кратеры были отождествлены и сосчитаны путем таких же методов как и те, которые употреблялись для составления каталогов лунных кратеров; особенное внимание было уделено классу и качеству кратеров. Подсчет кратеров с диаметром $D < 20$ км начинает указывать на эффекты незаконченности. Прямое изучение фотоснимков а также и постоянства пропорций класса кратеров в интервале диаметров кратеров больше 20 км указывает на то что существенная эрозия и сглаживание всех кратеров, за исключением наибольших, имело место в истории Марса. Эпохи образования кратеров и их эрозии кажутся тесно связанными во времени.

Программа статистического вычерчивания эмпирических кривых для наблюдаемых соотношений диаметра-частоты кратеров и дифференциального числа по закону распределения плотности AD^{-B} дает $B = 2{,}5 \pm 0{,}2$ для $D > 20$ км или $B = 3{,}0 \pm 0{,}2$ для $D > 30$ км. Население ударившихся предметов, считающихся причиной этих кратеров берется как имеющее дифференциальное число плотности, изменяющееся как $X^{-\beta}$ где X является диаметром ударившего предмета. Число „живых" комет и Аполло предметов, пересекающих орбиту Марса, является недостаточным на более чем два порядка величины для того чтобы объяснить наблюдаемое число плотности кратеров на Марсе. Для астероидальных предметов с $\beta = 2$ или 3, предсказанные и наблюдаемые числа плотности не могут быть согласованы без предположения о ранней эпохе очень высокой интенсивности образования кратеров на Марсе. Для $\beta = 4$ или 5, согласование между предсказанными и наблюдаемыми числами плотности может быть обеспечено с почти равномерной интенсивностью астероидальной бомбардировки. Отсутствие насыщенной бомбардировки Марса для очень больших кратеров указывает на величину β значительно большую 3. Это не является несовместимым с ожиданиями астероидов с $X > 1$ км во внутренней части астероидального пояса. В этом случае диаметр

кратеров соизмерим с кинетической энергией W, ударяющихся предметов, как $W^{1/3}$.

Для всех приемлимых величин β, разрушение вызваное ударом способствует эрозии и сглаживанию. Часть поверхности, покрытой кратерами, является величиной порядка единицы. Для всех приемлимых величин β, астероидальная бомбардировка может дать количественные данные о наблюдаемых величинах обоих A и B, в особенности если зона сглаживания вокруг кратеров Марса является большей, чем вокруг лунных кратеров. Для почти-насыщественной бомбардировки, существующие наблюдения являются очень мало способствующими определению величины β, или различию между насыщенной бомбардировкой и таковыми другими механизмами эрозии как выветренная пыль от удара или микрометеоритного происхождения; жидкая вода на широких или микрошкалах; строение гор; и затопление лавой. Пыль, произведенная ударами в течение истории Марса оценена как имеющая глубину между 0,1 и несколькими километрами. Диаметр наибольшего кратера сглаженного за $4{,}5 \times 10^9$ лет, согласно вычислениям, является между 60 и 180 км; для продолжительности жизни против эрозии, взятой как D^{α}, мы высчитываем $\alpha \simeq 0$ для $\beta = 2$ или 3, и $1 \leq \alpha \leq 2{,}5$ для $\beta = 4$ или 5.

Для $\beta < 3$ средний возраст кратеров на Марсе был найден приблизительно равным возрасту планеты. Несмотря на это, для β значительно большей чем 3, иные кратеры будут иметь иные возрасты, начитывающие от приблизительно $2{,}25 \times 10^9$ лет для самых наибольших кратеров и опадающие к нескольким миллионам лет или меньше для кратеров меньше чем в 20 км. В этом случае особенности поверхности порядка 10 км ширины или меньше могут быть довольно выделяющимися в ранней истории Марса и не обнаруживаемыми на фотоснимках Маринера 4. Итак, отсуствие таких знаков текущей воды как речные долины на фотоснимках Маринера 4 является совершенно не относящимся к делу в вопросе о существовании водяных тел в ранней истории Марса. Эти заключения о возрастах являются независимыми от оценок возрастов лунных морей. Существует некоторое слабое основание для корреляции между высокой плотностью кратеров и темными областями на Марсе.

AN ANALYSIS OF THE MARINER 4 PHOTOGRAPHY OF MARS

Clark R. Chapman, James B. Pollack, and Carl Sagan

1. INTRODUCTION

On July 15, 1965 (UT), the United States spacecraft Mariner 4 obtained, from a distance ~ 15,000 km, a sequence of 22 photographs of the surface of Mars. A preliminary discussion of the first 15 frames (frames 16 to 22 lacked usable contrast) was made by the experimenters (Leighton, Murray, Sharp, Allen, and Sloan, 1965) with particular emphasis laid on the statistics of the craters discovered in this pioneering mission. Their report was criticized and further discussed by others in a series of short reports (Anders and Arnold, 1965; Baldwin, 1965; Witting, Narin, and Stone, 1965; Öpik, 1965, 1966; Binder, 1966; Hartmann, 1966). We present here a new reduction of the photographic data with applications to the origin, age, and history of the craters.

This work was supported in part by Grant NGR 09-015-023 from the National Aeronautics and Space Administration.

2. A NEW REDUCTION OF THE CRATERING STATISTICS

Three basic sources were employed for the Mariner 4 photography: 1) several sets of 8.5- × 11-inch glossy prints of the digital-to-analog conversion kindly provided by the experimenters and the Jet Propulsion Laboratory; 2) a set of high-quality 3.5- × 3.5-inch positive transparencies of the same bit conversion prepared at the Jet Propulsion Laboratory and provided through the kindness of Dr. James Edson; and 3) a set of high-contrast positive transparencies prepared photographically by Mr. Charles Hanson of the Smithsonian Astrophysical Observatory from set 2 .

These sources were then used to compile a crater catalog. The preparation of such a catalog is a nontrivial task. The recent history of lunar crater studies provides several examples of incomplete or inexact crater counts leading to erroneous conclusions. In the case of the Mariner photographs, the difficulties are augmented by the poorer photographic quality, the generally small solar zenith angles, and problems in the connection of the photometric response of the video system for adjacent frames. One of us (CRC) has had experience in measuring and classifying lunar craters (Arthur, Agnieray, Horvath, Wood, and Chapman, 1963, 1964) and is primarily responsible for compiling the catalog of Martian craters (and possible craters) presented as Appendices A and B. The other two authors have checked these identifications. There is always the danger in such a catalog that spurious craters may be listed, but a catalog that includes only the entirely unambiguous features can be very misrepresentative — especially in the present case of small solar zenith angles, relatively poor contrast discrimination, and heavily eroded craters. Thus, while we have included a feature only when there appears to be good indication from several lines of evidence that it is indeed a crater (such criteria as circularity and appropriate illumination were weighted heavily), there may be several objects listed that are not true craters. The column of the catalog headed "quality" distinguishes unambiguous from ambiguous craters. For all of the analyses

based on this catalog, the doubtful objects will be ignored. Although the best frames have a ground resolution of under 4 km, there are relatively few entries in the catalog with diameters < 10 km, owing to the poor quality and poor visibility of the smaller craters. However, close inspection of the best transparencies gives the distinct impression of many small craters slightly larger than the limiting resolution (a few scan lines across). Representative diagrams, showing the approximate positions and qualities of craters in selected frames, are displayed in Figures 1, 3, and 5. The corresponding photographs are duplicated in Figures 2, 4, and 6. Many of the craters are visible only on the original transparencies and prints, and not in halftone reproductions. Therefore, we have not reproduced the entire set of Mariner 4 photographs here. The experimenters have called the usable frames "Pictures," and have numbered them sequentially.

Table 1 summarizes the relevant parameters for each usable frame. The photographic-quality entry is a subjective measure of the clarity of a given picture, assuming that the region of the Martian surface in question has a well-defined intrinsic contrast. Among possible reasons for a variation in quality from frame to frame are the solar-illumination angle, the photometric-function program of the video system, surface erosion, and overlying clouds. A. Dollfus (1965, private communication) reports obscuration by white clouds of the region of Pictures 12 to 15 a few days before encounter. The resolution is displayed in Table 1 as kilometer per line — the surface displacement corresponding to the video line separation. For pictures of "very good" quality, the catalog is probably complete down to craters a few resolution elements across, at least for the less eroded craters. Considerable loss in completeness — particularly for craters of small diameter — can be expected for pictures where the quality is only "fair." Rounded-off estimates of the dimensions and areas of the Martian surface regions viewed in each picture, and the color filter used, are also displayed in Table 1.

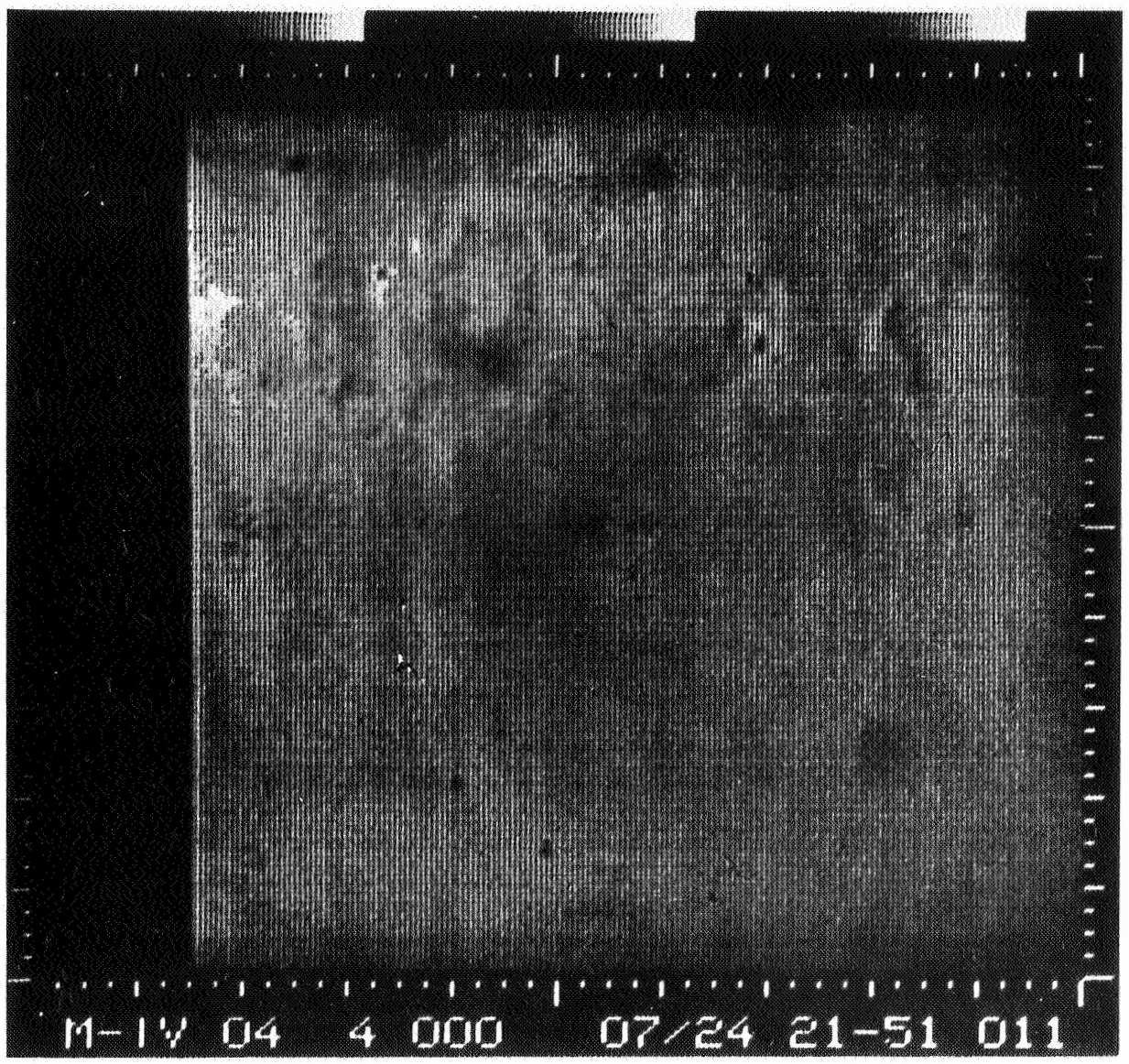

Figure 1. Low-quality reproduction of Picture 4 of the Mariner 4 photographic sequence.

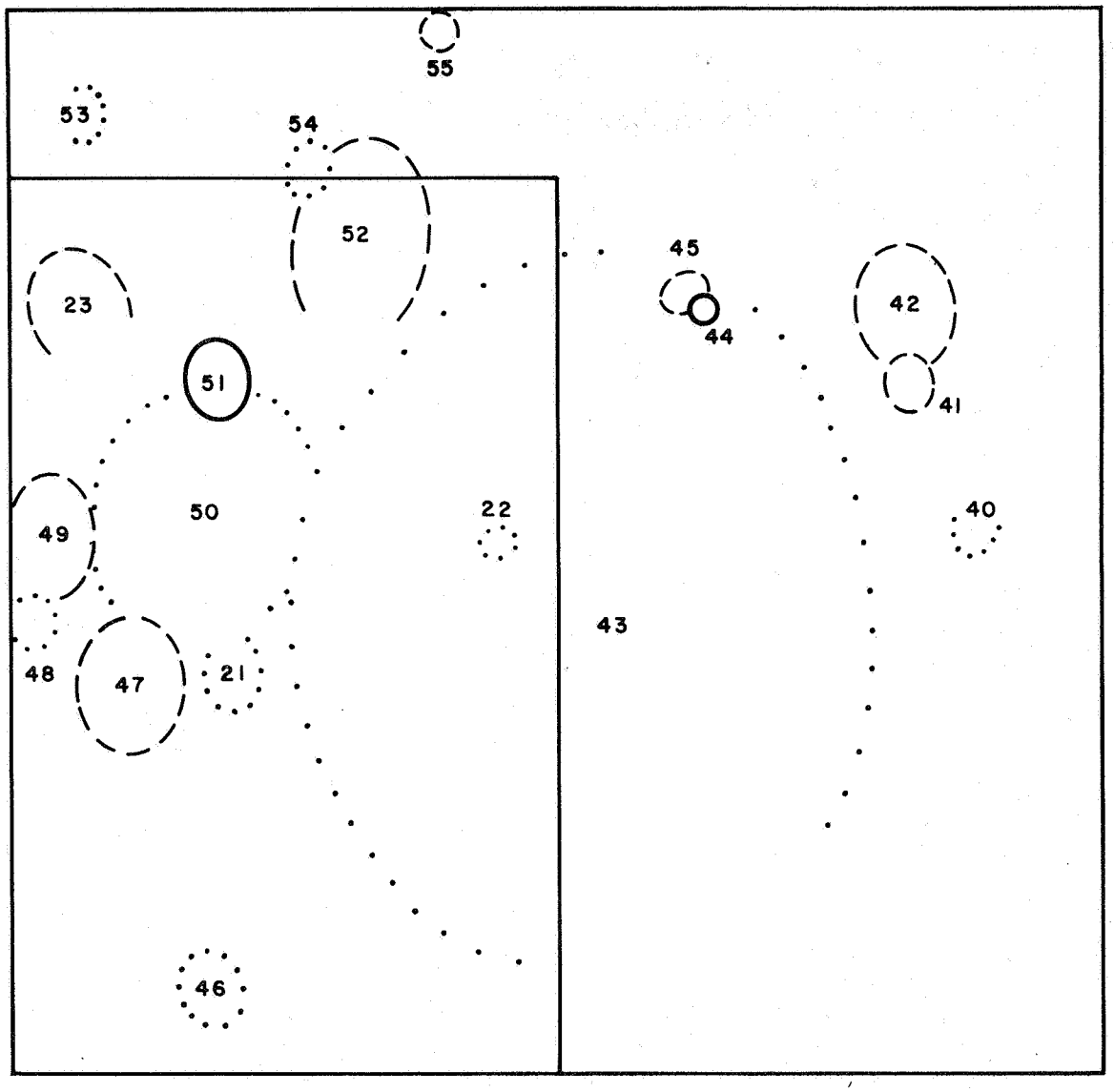

Figure 2. Sketch of the position of cataloged craters (Appendices A and B), Picture 4 of the Mariner 4 photographic sequence.

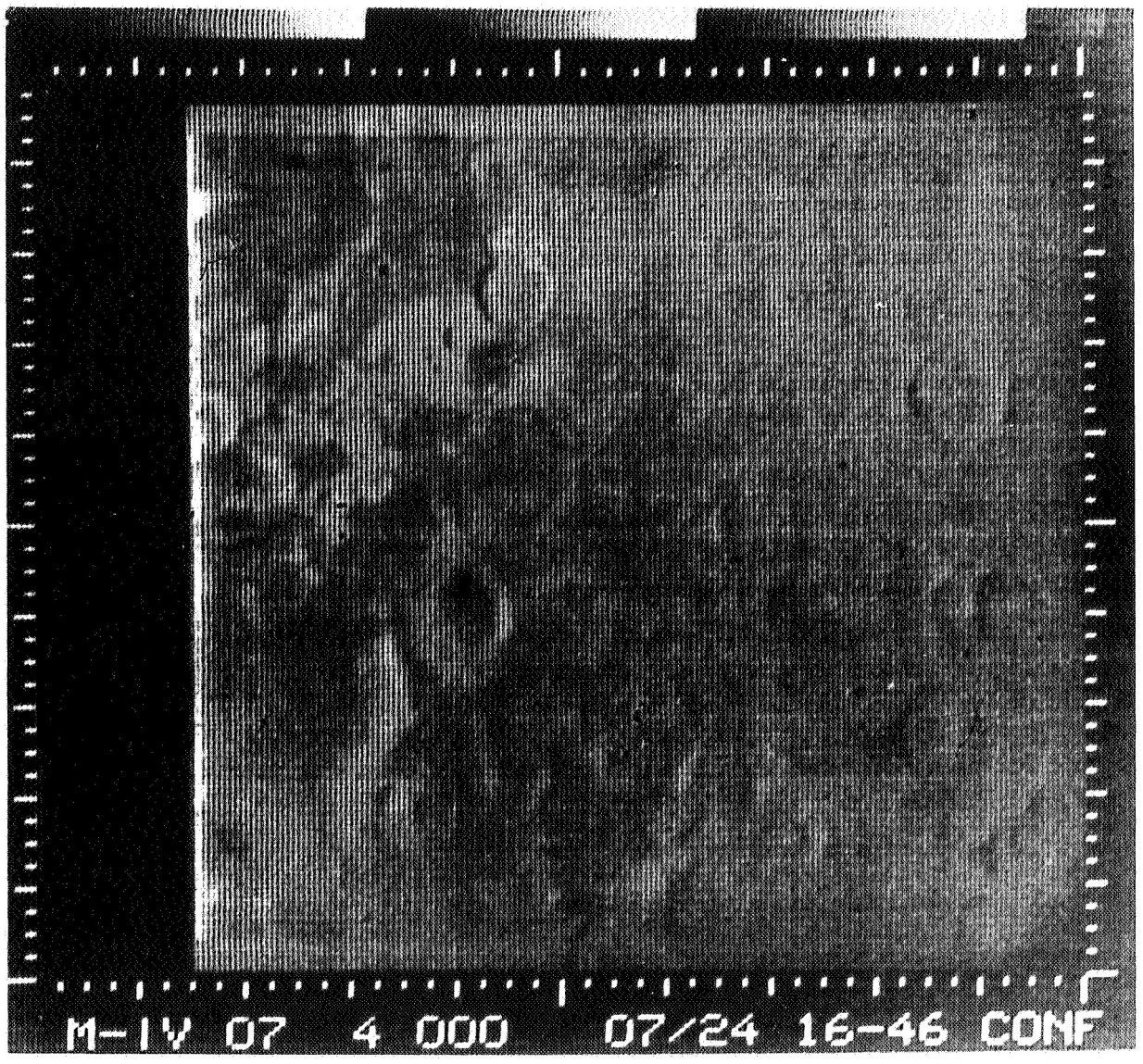

Figure 3. Low-quality reproduction of Picture 7 of the Mariner 4 photographic sequence.

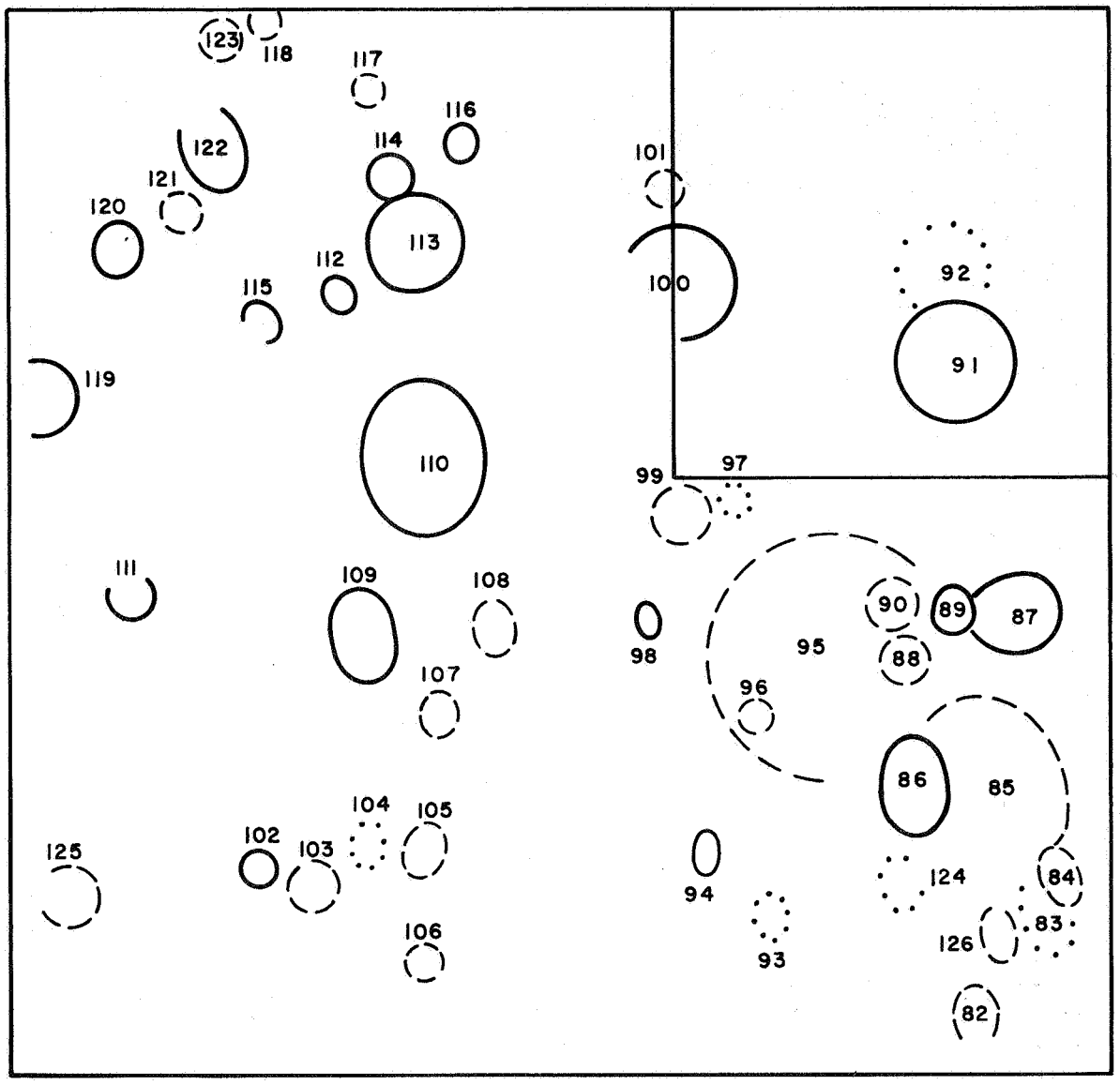

Figure 4. Sketch of the position of cataloged craters (Appendices A and B), Picture 7 of the Mariner 4 photographic sequence.

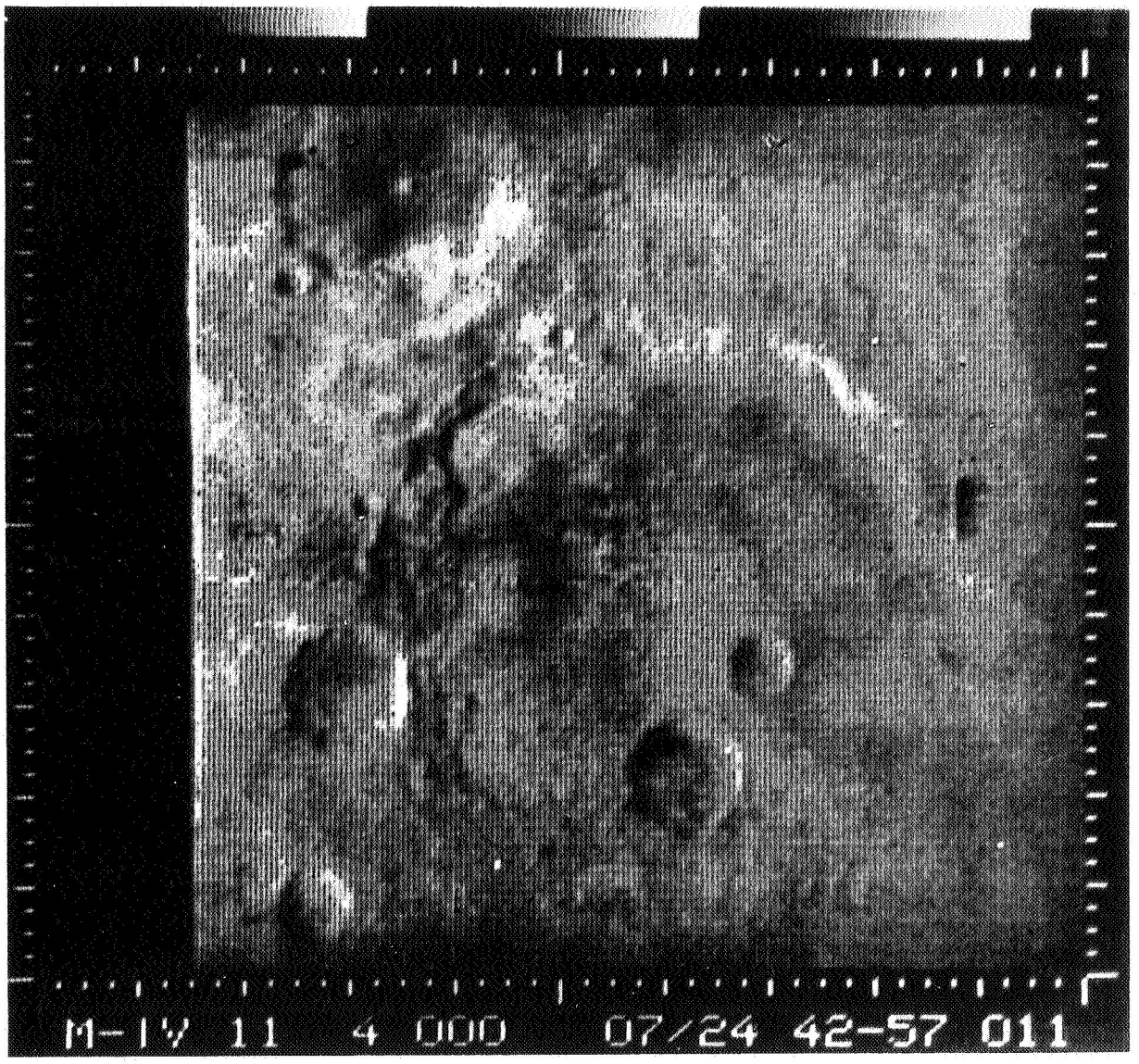

Figure 5. Low-quality reproduction of Picture 11 of the Mariner 4 photographic sequence.

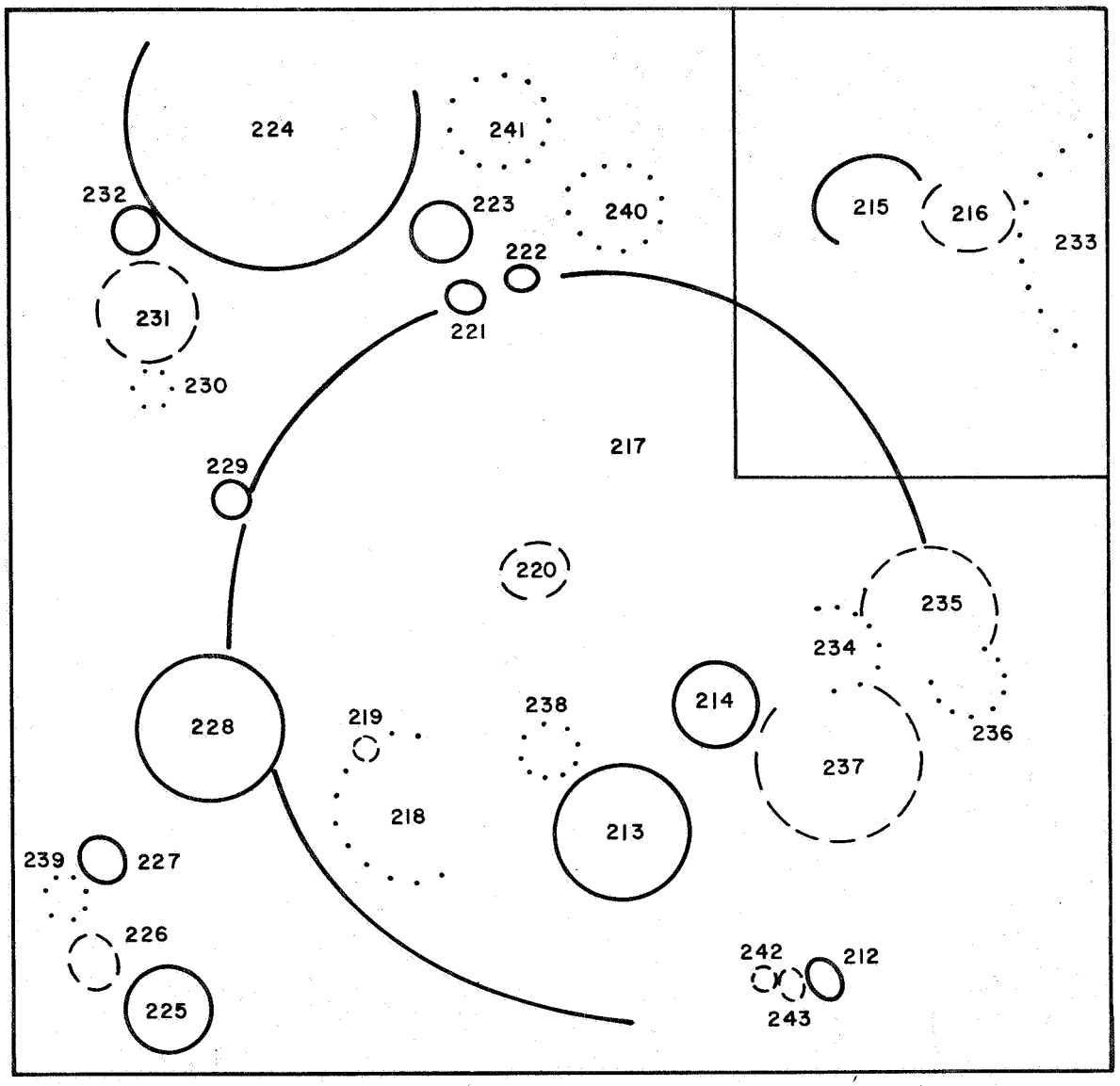

Figure 6. Sketch of the position of cataloged craters (Appendices A and B), Picture 11 of the Mariner 4 photographic sequence.

Table 1. Parameters of Pictures 2 to 15 of the Mariner 4 photography

Picture	Dimensions (km) E-W	Dimensions (km) N-S	Area (km^2)	Filter	Solar altitude	Quality	km/line
2	470	850	398,000	green	70°	fair	5.2
3	350	500	177,000	green	76°	fair	3.1
4	340	430	147,000	orange	76°	fair	2.7
5	310	350	108,000	orange	71°	fair	2.1
6	310	320	99,000	green	68°	fair	2.0
7	290	290	84,000	green	51°	very good	1.8
8	290	270	80,000	orange	58°	good	1.7
9	270	260	70,000	orange	52°	good	1.6
10	270	260	70,000	green	49°	good	1.6
11	270	240	66,000	green	43°	very good	1.5
12	270	240	66,000	orange	40°	fair	1.5
13	270	230	62,000	orange	33°	fair	1.4
14	270	230	62,000	green	30°	fair	1.4
15	290	230	65,000	green	24°	fair	1.4

The catalog in Appendices A and B presents all clear craters, and many additional ambiguous crater-like objects, on Pictures 2 through 15. Because Pictures 2 through 6 are of generally poorer quality (cf. Table 1), craters in those pictures have been separately listed in Appendix A. Craters in Pictures 7 through 15 are listed in Appendix B. The reliability of crater identification is much higher for Appendix B than for Appendix A. A sequence number, 1 to 298, is assigned to each entry. After iteration in compiling the catalog, a few entries have been dropped upon closer scrutiny; as a result, some sequence numbers (e. g., 124) do not correspond to probable craters. When a crater appears in the overlap region of two adjacent frames, separate values are listed under the same sequence number; in later data reduction such craters are counted only once. The approximate positions of craters in the catalog are distances in centimeters from the south and west edges of the 8.5- × 11-inch prints distributed by NASA, and are intended for orientation of the reader interested in comparing his prints with the catalog. Crater diameters displayed were measured in the unforeshortened direction and are uncertain to a few kilometers.

There are uncertainties in the reliability of identification of features from frame to frame, and within a given frame. A qualitative measure of this reliability is a parameter we call crater quality, to be distinguished from the picture quality of Table 1. Factors affecting crater quality include picture quality, solar zenith angle, crater diameter, and crater class (see below). Quality A objects are definitely craters. Quality B objects are definitely Martian surface features, and are probably craters. Quality C objects may be craters. Some more-or-less circular features were omitted because of positive identification as photographic defects, or because the lighting was not that expected for a crater with the known solar illumination. Because of the relative clarity of lunar photography, it is not customary to introduce a crater-quality parameter in lunar studies.

To be distinguished from crater quality is a parameter called crater class, which is customarily employed in lunar studies. The classifications 1 through 4 are an index of crater morphology. For Martian craters we find

(as for lunar and terrestrial craters) a continuous spectrum of crater forms, varying from fresh, sharp, circular, deep craters with concave floors and raised rims (Class 1) to features so severely deformed or eroded as to be barely recognizable as craters (Class 4). If large-scale Martian craters are produced by hypervelocity impact of asteroidal and cometary debris, then they must have all begun as Class 1 craters, subsequently undergoing processes of deformation and erosion leading to craters of higher class. Similar classification schemes are widely used in lunar studies (Young, 1940; Baldwin, 1963; Arthur et al , 1963, 1964; Arthur, Agnieray, Horvath, Wood, and Weller 1965; Arthur, Pellicari and Wood, 1966; Hartmann, 1965), and have proved useful despite the differences among classification schemes.

The four classes employed in the present study are defined as follows:

Class 1: These fresh, uneroded craters are characterized by a prominent raised circular rim, a concave floor, and no appreciable softening or overlapping by other craters.

Class 2: These craters are somewhat less perfect and prominent than those of Class 1. They have complete, relatively high walls, although some degree of softening and slumping may be evident. The central portions of the floor may be flattened, although much of the interior of the crater remains bowl-shaped. There may be some overlapping by small craters.

Class 3: These craters have flat floors. The walls are considerably lower in proportion to the crater diameter than for Classes 1 and 2, but they are still quite apparent and more or less complete. The crater may show some departure from circularity and may be overlapped. Its features may appear somewhat softened.

Class 4: These craters have very low walls, often with large portions barely distinguishable or missing. The floors are entirely flat. The crater may show considerable departures from circularity and is very battered and eroded, marked by much softening of detail, filling, and overlapping.

This classification is comparable to that of Arthur et al. (1963, 1964, 1965, 1966), with the exception that Class 5 is here omitted. This class includes craters so severely destroyed as to be marginally visible, even on the best lunar photographs taken at large solar zenith angles. Similar Martian craters – in the few instances that they are detectable – are included as Class 4 objects in the present catalog. With this exception the present classification should be quite comparable with that of Arthur et al.
In classifying Martian craters, comparison was made with lunar craters on photographs with similar solar zenith angles. The same standards, based on the distribution of brightness over the crater, were used to determine Martian crater characteristics as are routinely used in lunar studies. One of the principal applications of the catalog, presented below, is an analysis of erosion on the Martian surface. To treat this problem conservatively, craters were generally given the lowest classification consistent with their appearances – i.e., the effect of solar illumination was slightly over-compensated for.

The classification scheme presented here should be largely independent of such factors as crater diameter and solar zenith angle; the vast majority of classifications fall on a relative scale that should be duplicated by any independent classifier attempting to follow the class definitions above.
In making the absolute classifications, we have assumed that the prevailing Martian terrain is not very rugged, consistent with the low general slopes deduced from radar Doppler spectroscopy (Sagan, Pollack, and Goldstein, 1967). Some craters were not classified on the early frames because of difficulties introduced by the high altitude of the sun.

After completion of the catalog and analysis of the present paper, a preliminary announcement was made of the production of electronically dodged, contrast-enhanced Mariner 4 frames, prepared by the experimenter team (Leighton, 1967). The total number of fairly unambiguous craters detected on the new frames is about 300, very close to the number of craters reported in the catalog of the present paper. For this reason, and for

reasons discussed above and below, we believe that the analysis of the present paper does not require significant modification because of the new photographic reduction.

3. CRATER EROSION AND OBLITERATION

We assume that the large detectable Martian craters are of impact origin, as is generally believed to be true for lunar craters of comparable size.

An inspection of the crater catalog (Appendices A and B) reveals that a significant fraction of the craters belongs to Classes 3 and 4. For example, of the 53 Quality-A and-B craters on Pictures 7 through 14 with diameters larger than 20 km, 87% are members of Class 3 or 4. Since all impact craters would initially belong to Class 1, we conclude that many craters have been significantly modified or eroded since their time of formation; they have been largely filled in and in some cases their ramparts have been breached.

It is natural to ask at this point whether some craters have been so severely damaged as to be indetectable on the Mariner 4 photographs. An inspection of Crater 217 of Picture 11 suggests that some of the smaller craters would be almost completely obliterated. If a crater 150 km in diameter can be significantly eroded (among other criteria, its western ramparts are entirely missing), then smaller craters of a similar or greater age may be entirely expunged. In the following discussion we will distinguish between erosion and obliteration, defined as above.

To explore this matter in greater detail, we have determined the fraction of craters in each class for several diameter intervals. The data are presented in Table 2. Below about 20 km, incompleteness sets in for the later classes, a point to which we will return shortly. We see that for the diameter interval above 20 km, the class percentages are remarkably similar. This suggests a common erosion history for craters of diameter larger than 20 km, and permits us to use the extensive erosion of the larger craters to infer obliteration of the smaller craters.

Table 2. Crater percentages by class at several diameter intervals for Mars and the Moon

Region	Class	Diameter interval (km)					
		5-10	10-15	15-20	20-30	30-60	>60
Mars, Pictures 7-14, Quality A and B	1	38	11	14	4	4	0
	2	58	26	24	9	8	14
	3	2	43	29	46	34	43
	4	2	20	33	41	54	43
Lunar Highlands (selected pure continental regions)	1	18	17	14	7	1	4
	2	25	23	26	27	19	12
	3	44	35	24	24	25	32
	4	13	25	36	42	55	52

The near constancy of class membership for different diameter intervals above 20 km can be used to establish a lower bound on the size at which obliteration begins. Let $t_i(D)$ represent the lifetime of a crater of diameter D and class i. If the erosion processes have time-invariant rates, the ratio of the time spent as a crater of class i to that spent as a crater of class j, $t_i(D)/t_j(D)$, will equal the observed ratio of membership in the two classes, which may be found from Table 2. If D^* represents the maximum diameter of craters that suffer obliteration, then $\Sigma_{i=1}^{4} t_i(D^*)$ will equal the time scale during which erosion occurs. For craters with diameters exceeding D^*, there will be relatively fewer belonging to Class 4, and the fraction of Class 4 objects will be given by

$$f_4(D) = \frac{\sum_{i=1}^{4} t_i(D^*) - \sum_{i=1}^{3} t_i(D)}{\sum_{i=1}^{4} t_i(D^*)}$$

$$\text{for} \sum_{i=1}^{4} t_i(D^*) \geq \sum_{i=1}^{3} t_i(D) \quad ;$$

$$f_4(D) = 0$$

$$\text{for} \sum_{i=1}^{4} t_i(D^*) < \sum_{i=1}^{3} t_i(D) \quad . \tag{1}$$

Similar results will apply even when the erosion rates are time variable.

We now express equation (1) in a more useful form. Suppose $t_1(D)$ scales as D^a, for $D < D^*$. Table 2 implies that $t_i(D)/t_j(D)$ is independent of D for $D < D^*$, and so all $t_i(D)$ will scale as D^a for $D < D^*$. Furthermore, whenever $f_4(D) > 0$ such a scaling will be preserved for Classes 1 through 3. Thus equation (1) becomes

$$D^* = D \left\{ \frac{\sum_{i=1}^{3} t_i(D^*)}{[1 - f_4(D)] \sum_{i=1}^{4} t_i(D^*)} \right\}^{1/a} \quad . \tag{2}$$

The ratio of the summations over $t_i(D^*)$ as well as $f_4(D)$ can be obtained from Table 2; D^* can then be obtained from equation (2) for a given choice of D and α. Since the class membership for craters larger than 60 km was based on only seven craters, the uncertainty in $f_4(D)$ may be (as much as) a factor of 2. Any deviation from constancy for class proportions is expected only for the largest craters, because the statistics are good except for $D > 60$ km. Taking $D = 90$ km, an average value for the range $D > 60$ km, and $f_4(D)$ as one-half the value relevant for the smaller craters, we obtain a lower limit on D^*, D^*_{min}; i.e., D^*_{min} is the smallest possible diameter of a crater so large that obliteration is becoming ineffective. The resulting values of D^*_{min} are given in Table 3 for various choices of α. We show in Sections 4 and 6 that the values of α given in Table 3 cover the plausible range.

Just as D^* measures the largest diameter at which obliteration is effective and at which the percentage of Class 4 craters equals the equilibrium value, D'_j measures the diameter at which class j ceases to contain the equilibrium number and has fewer members. The relevant equation for D'_j is given by setting the total erosional time, $\Sigma_{i=1}^{4} t_i(D^*)$, equal to the time for an early crater of diameter D′ to just cease being a class j object, $\Sigma_{i=1}^{j} t_i(D')$. The results are shown in Table 3 for Classes 2 and 3, where D^*_{min} was used to estimate D^*. Equilibrium values for these classes, as well as for Class 1, will therefore hold for diameters comparable to or larger than the ones listed in the crater catalog.

Table 3. Minimum diameters for obliteration and equilibrium class membership

α	D^*_{min}	$D'_{3\ min}$ (km)	$D'_{2\ min}$
2	75	103	200
1	62	117	477
1/2	43	152	2,540
1/4	21	263	73,000

The value of D^*_{min} for $\alpha = 1/4$ is actually too small, since this would lead to $f_4(D) = 0.25$ for the diameter interval 30 to 60 km. Such a value is in contradiction to the data for this interval in Table 2, which are based on 24 craters. Furthermore, with the exception of the case $\alpha = 0$, all plausible erosional mechanisms can be expected to have $\alpha \geq 0.5$. Thus, 43 km will be a lower limit to D^*. In the $\alpha = 0$ case, discussed below, there of course need not be any obliteration.

Hartmann (1966), Binder (1966), and Öpik (1966) have claimed that obliteration sets in at about 50 km, 40 km, and 20 km, respectively. They base this conclusion on finding fewer craters below these diameter limits than would be implied by a simple extrapolation of the diameter-frequency relation for the larger sized craters. Hartmann's and Binder's results actually do not clearly indicate a deficiency except for craters with diameters below about 20 km. We believe these deficiencies may have been influenced by observational incompleteness. While the sharp Class 1 objects can be observed down to such small diameters as a few kilometers, as limited by the resolution of the video system and the quality of the picture, the later class craters will show incompleteness at larger diameters. Table 2 illustrates this point: Between 5 and 10 km, only 4% of the craters in the catalog are of Class 3 or 4. There seems to be some incompleteness up to at least 20 km. Since Class 3 and 4 craters constitute a major fraction of the larger craters, their incompleteness at smaller diameters could easily lead to the effect found by Hartmann, Binder, and Öpik. Furthermore, we have included less obvious craters than have these two authors.

[Note added in proof: Leighton, Murray, Sharp, Allen, and Sloan (1967), from a study of the Mariner 4 vidicon-response function and particularly from a study of plaster-of-paris models of craters photographed with the Mariner 4 system, deduce a real discontinuity at about 20 km. However, their crater models are of well-preserved (Class 1 and 2) craters, not of the more poorly preserved craters that suffer incompleteness earlier. In examining the results of Leighton, et al., find that a bend in the

diameter-frequency curve begins at about 30 km or slightly larger diameters. We suspect that this difference is due in part to the inclusion by Leighton, et al., of the frames of poorer quality. For these reasons and for the additional reasons mentioned above, we are not persuaded that a 20- or 30-km break is real.]

The percentages of craters by class also permit us to make a rough comparison between the times of the last significant erosion and the last important epoch of crater formation. The existence of many badly damaged craters implies erosion could not have stopped until close to or after crater formation ended (or at least greatly slowed down). The presence of some craters of Classes 1 and 2 shows that erosion could not have continued long after the last period of bombardment. This conclusion is, of course, compatible with, although not uniquely indicative of, a uniform rate of crater formation and erosion, continuing to the present. It is also compatible with saturation bombardment as the principal crater-erosion mechanism.

In summary, many of the observed craters have been severely eroded; and, except for one choice of α, complete obliteration of the oldest craters smaller than 43 km and perhaps of some larger during the history of Mars is inferred. Crater formation and erosion appear to be closely tied together in time.

4. SOURCES OF IMPACT CRATERS

We will attempt to find the most abundant source of impacting objects and see to what extent it can account for the observed number of Martian craters.

Kuiper (1959), Öpik (1960), and others have suggested that some of the large lunar craters, particularly in the maria areas, can be attributed to cometary impact. Some of these comets are "dead" short-period comets consisting only of nuclei that have survived disintegration due to heating, outgassing, tidal interaction, etc. An upper limit on the number of such comets can be found by considering all members of the Apollo group to be "dead" comets. Apollo objects are the largest bodies known to cross the orbit of the Earth. Of the eight observed members, seven have diameters exceeding 1 km. Opik (1963) points out that, owing to observational incompleteness, the actual number of Apollo members with a diameter in excess of 1 km may be about 40. Öpik also estimates from the observations that there may be twice as many "live" comets crossing the Earth's orbit with diameters in excess of 1 km. Many of these live comets may be destroyed in passing through a planetary atmosphere. Thus, an upper limit (and perhaps a generous one) to the number of Earth-crossing comets with diameters in excess of 1 km and capable of producing large craters is about 100. A similar figure will hold for the number of Mars-crossing comets; furthermore this figure should be fairly constant with time.

A second source of impacting bodies on Mars is Mars-crossing asteroids that derive from the asteroid belt located between the orbits of Mars and Jupiter. There are 10 observed Mars-crossing asteroids with diameters larger than 20 km. The number of asteroids with diameters between X and X + dX, where $X > 20$ km, is given approximately by a power law dependence:

$$n(X)\,dX = 200\,X^{-2}\,dX, \qquad X \text{ in km}, \quad X > 20 \text{ km} \tag{3}$$

(cf. Öpik 1963). For diameters smaller than 20 km, incompleteness sets in, and it is not necessarily valid to assume that n(X) will continue to scale as X^{-2}.

In extrapolating n(X) as $X^{-\beta}$ from 20 km to 1 km, the values of 2 and 5 are probably extreme limits to the value of the exponent. Kuiper et al. (1958) found the exponent β ranging from 2.8 to 4.6 depending on the position of the asteroid in the asteroid belt for objects with diameters between about 5 km and 20 km. More recent work, still unpublished, by C. J. and I. van Houten (G. P. Kuiper, private communication, 1965) suggests a value of 2.9. Large incompleteness corrections are involved in this work. The asteroids impacting Mars and causing the craters observed by Mariner 4 will be smaller than the usual asteroids observed from the Earth, and will arise preferentially from the inner part of the asteroid belt. Both circumstances should lead to a higher value for the size-distribution exponent, β, than applies to the observed asteroids as a whole: Small asteroids have probably been involved, on the average, in more collisions than large asteroids and should therefore be characterized by larger values of β. Grinding of quartz in mills for some hundreds of hours produces a distribution function with β approaching 4 (Gaudin, 1944) and monotonically increasing with time. More prolonged grinding may produce even larger values of β. Hawkins (1960) concludes that both asteroid and meteoritic observations are consistent with $\beta \simeq 4$. In order to understand the short cosmic-ray exposure ages of chondrites, Arnold (1965; see also Wetherill, 1967) was forced to postulate β approaching 4 for $X < 6$ km. Mars-crossing asteroids that originate from the center of the asteroid belt have also probably encountered more collisions than asteroids with present orbital positions near the center of the belt; and, by the same argument, larger β should prevail for them. Some evidence for such a dependence of β on X and position has, in fact, been presented (Kuiper, Fugita, Gehrels, Groeneveld, Kent, van Biesbroeck, and van Houten, 1958), but further work is clearly needed. In any case, we expect that β for our problem

will be larger than the mean values usually quoted. We will suppose initially that, between 20 km and 1 km, n(X) scales somewhere between X^{-2} and X^{-5}:

$$n(X) = k_1 X^{-\beta}, \quad 5 \geq \beta \geq 2, \quad X < 20 \text{ km} \quad . \tag{4}$$

The constant k_1 may be found by demanding that equations (3) and (4) agree at X = 20 km. In this way we find k_1 to be 8.93×10^2 for $\beta = 2.5$ and 3.57×10^5 for $\beta = 4.5$, for X measured in kilometers. The number of Mars-crossing asteroids at the present time with diameters in excess of 1 km is found by integrating n(X) from unity to infinity. The result, N(X > 1 km), is 6.0×10^2 for $\beta = 2.5$ and 1.0×10^5 for $\beta = 4.5$.

We next attempt to find the number of craters produced by cometary and asteroidal objects in $T_{\sigma} = 4.5 \times 10^9$ years, the approximate age of Mars, and compare this figure with the observed number of craters. We assume initially that the present distribution of impacting objects is representative of the entire planetary history, an assumption good for the comets and more problematical for the asteroids.

The relevant equations for the production of craters by impacting objects has been given in many places (see, e.g., Baldwin, 1963), and we summarize them here. The crater diameter, D, produced by an object of diameter X, is related to the kinetic energy, W, of the impacting object:

$$D = k_2 W^{1/\nu} = k_2 \left[\frac{1}{2} \left(\frac{\pi \rho X^3}{6} \right) V_t^2 \right]^{1/\nu} , \tag{5}$$

where ρ is the density of the impacting object and V_t its velocity immediately before impact. The constant k_2 is usually estimated from the size of craters produced by manmade, particularly nuclear, explosions of known energy, and equals approximately 8×10^{-2} when D is in kilometers and W in kilotons of TNT equivalent (4.19×10^{19} ergs) (Shoemaker, Hackman, and Eggleton, 1961); k_2 depends only slightly on the choice of ν.

The best estimates of ν lie between 3 and 3.6 (Shoemaker et al., 1961; Baldwin, 1963). The reader is cautioned, however, that these values of ν are based primarily upon terrestrial explosions of much smaller energies than the ones of interest in the present discussion. Note that when $\nu = 3$, $D \propto X$.

The value of V_t is related to V_∞, the relative velocity of the impacting object and Mars at a large distance from the planet, and to V_e, the escape velocity, by energy conservation: $V_t^2 = V_\infty^2 + V_e^2$. For Mars, V_e is 5.1 km sec^{-1}, and V_∞ has an average value of about 10.5 km sec^{-1} for the Mars-crossing asteroids and a similar value for the comets (Öpik, 1963). Thus V_t is approximately 11.5 km sec^{-1}. We choose $\rho = 7.8$ g cm^{-3} for the asteroids, a density typical of iron-nickel meteorites, and $\rho = 1/2$ g cm^{-3} for the comets.

We now relate the number of potential impacting bodies to the number of craters they will produce. The number of impacts per unit time involving objects with diameters in excess of X_c equals the number of such objects divided by their lifetime against impact, t_{σ}:

$$\int_{X_c}^{\infty} n(X) \frac{dX}{t_{\sigma}} \quad .$$

This, in turn, will equal the number of craters formed in 4.5×10^9 years,

$$\int_{D_c}^{\infty} n_f(D)\, dD \quad ,$$

divided by $T_{\sigma} = 4.5 \times 10^9$ years:

$$\int_{D_c}^{\infty} n_f(D) \frac{dD}{T_{\sigma'}} = \int_{X_c}^{\infty} n(X) \frac{dX}{t_{\sigma'}}$$

$$= \frac{N(X > X_c)}{t_{\sigma'}} \quad . \tag{6}$$

Here, D_c is the diameter of a crater produced by an impacting object of diameter X_c; $n_f(D)\,dD$ is to be distinguished from $n(D)\,dD$, which is the frequency relation for currently observed crater numbers between D and D + dD on the entire Martian surface; $t_{\sigma'}$ is approximately 7.4×10^9 years for asteroids and about half this figure for comets (Öpik, 1963).

A statistical curve-fitting program for crater diameter-frequency relations, derived by Chapman and Haefner (1967) for the Moon, is here applied to Mars. We use differential rather than cumulative crater frequencies. The number of craters on Mars having diameters within a 1-km diameter increment centered on D is expressed as $n(D) = AD^{-B}$; values of A and B can then be derived by use of the data in the crater catalog of the appendices. The parameters A and B vary to some extent with crater diameter, crater class, and quality; but after extensive study, we have found that generally the crater sample is too small to allow reliable estimates of these variations. If future photographic missions to Mars (such as the projected 1969 Mariner) can obtain five times better surface coverage with the same or improved resolution, much more refined statistical analyses will be possible.

The weighting in the curve-fitting procedure allows for the differing number of points in each diameter increment, which gives greater weight to smaller diameters where craters are most numerous. Therefore, it is crucial to determine the maximum diameter at which some observational incompleteness exists. In general, we believe the crater sample is complete above 20 km, but we cannot rule out the possibility of some loss of Class 4

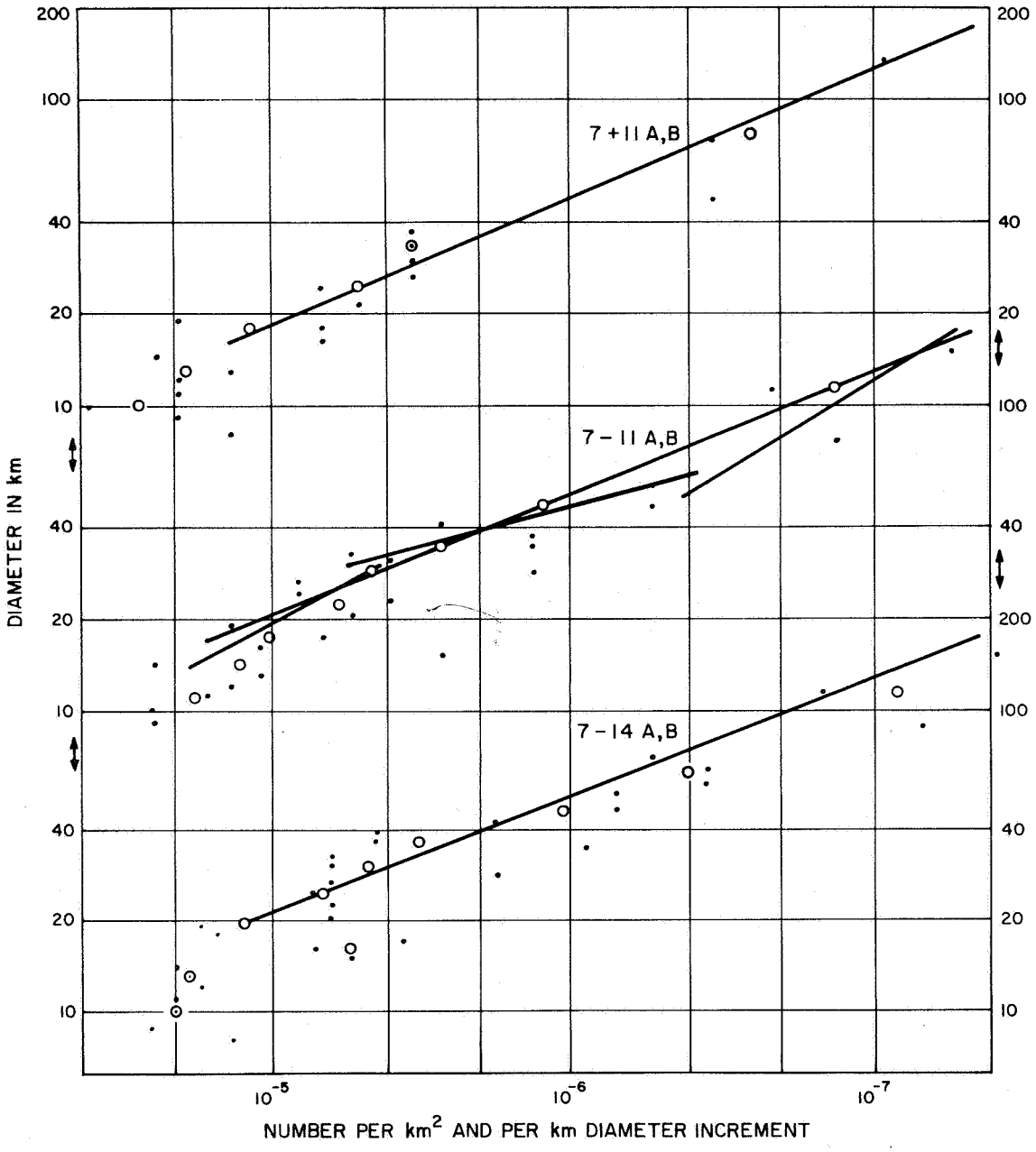

Figure 7. Diameter-frequency plot for Pictures 7 through 14, Qualities A and B (left);Pictures 7 to 11, Qualities A and B (center); and Pictures 7 and 11, Qualities A and B (right). The dots are the original counts; the circles are these counts grouped by threes; the straight lines represent increment-weighted least-squares fits. The incompleteness of the crater counts for D less than 20 km is particularly evident for the left-hand plot.

craters between 20 and 30 km; hence, we will carry two diameter-frequency relations as representing the observations (Pictures 7-14, Qualities A and B only):

$$A = 2.0 \times 10^6 \pm 1.2 \times 10^6, \qquad B = 2.5 \pm 0.2 \qquad \text{for } D > 20 \text{ km} \tag{7a}$$

$$A = 1.6 \times 10^7 \pm 1.3 \times 10^7, \qquad B = 3.0 \pm 0.2 \qquad \text{for } D > 30 \text{ km}, \tag{7b}$$

in units where D is measured in kilometers. The errors represent one standard deviation. In Figure 7 we show the diameter-frequency relationship for Pictures 7 through 14, Qualities A and B; Pictures 7 through 11, Qualities A and B; and Pictures 7 and 11, Qualities A and B. The solid lines are weighted least-squares fits.

[Note added in proof: The recent discussion by Leighton et al. (1967) implies $B \simeq 3.2$ for $D > 30$ km, in good agreement with our results.]

The current values, A and B, are to be distinguished from the fictitious values, A_f and B_f, for craters formed in the absence of obliteration due to any source, including crater overlap. Note that if $n_f(D) \propto D^{-B_f}$, and $n(X) \propto X^{-\beta}$, then from equations (5) and (6)

$$B_f = 1 + \frac{\nu}{3}(\beta - 1) \quad . \tag{8}$$

Thus, $\beta \leq B_f$. When $\nu = 3$, $B_f = \beta$.

Equations (3), (4), (5), and (6) are now employed to compute the number of craters produced by cometary and by asteroidal impact. The value of X_c is taken as 1 km for the comets; the values of $N(X \geq X_c)$ have been given above. There are 53 observed craters of Qualities A and B located on Pictures 7 through 14 (5.6×10^5 km^2) with diameters greater than or equal to 20 km, or about 1.4×10^4 such craters on all of Mars. By equation (7a), the corresponding number of craters larger than D_1 can be found from the scaling law $N(D > D_1) \propto D_1^{-1.5}$. Alternatively, to be conservative about incompleteness, we note that there are 32 craters with $D > 30$ km, and we can use equation (7b), finding $N(D > D_1) \propto D_1^{-2}$.

Table 4 compares the currently observed number of craters, $N(D > D_c)$, extrapolated to the entire Martian surface, with the corresponding number expected from cometary and asteroidal impacts. The observed number is actually a lower limit to the number produced, since, as we saw earlier, some craters may have been obliterated. We see that the comets produce far too few craters; as pointed out above, their present number is probably a good indication of the number of comets in the past. For $\beta = 2.5$, the asteroidal production of craters can be made to agree with the observed number of craters by demanding that there were more asteroids in the past then in the present; e.g., we could require ~ 500 times the present rate of asteroidal bombardment for the first 5×10^8 years of Martian history. Such a strategy has been adopted by Öpik (1966), who considers this demand most likely met by having many planetesimals present when Mars was first formed. If such planetesimals had inclinations $< 10°$ and semimajor axes similar to those of Mars, their lifetimes would be short compared to 4.5×10^9 years, and few of them would be left today. The idea of an early local population of impacting objects in the case of the Moon has been suggested by Kuiper (1954), by Urey (1962), and by Levin (1963). With Öpik's calculations, based on the less complete initial estimate of crater density made by the Mariner 4 experimenters, there was a factor-of-5 discrepancy between theory and observation on the assumption of uniform cratering rates. Our more complete counts show a discrepancy by a factor of about 50. But since we know very little about the formation of planets, very high initial bombardment rates cannot be excluded. Similar results hold for $\beta = 2.25$, which corresponds to $B_f = 2.5$ and $\nu = 3.6$. These two cases are equivalent to $B_f = \beta$.

Table 4. Comparison of predicted and observed numbers of Martian craters

Source	β	ν	D_c	X_c	Predicted $N(X > X_c)$	Observed $N(D > D_c)$ Eq. (7a)	Eq. (7b)
Comets	-	3	12.8 km	1 km	$\leq 1.2 \times 10^2$	2.9×10^4	6.6×10^4
Comets	-	3.6	5.5	1	$\leq 1.2 \times 10^2$	9.3×10^4	3.6×10^5
Asteroids	2.5	3	20	0.62	7.5×10^2	1.35×10^4	2.7×10^4
Asteroids	2.5	3.6	20	1.55	1.9×10^2	1.35×10^4	2.7×10^4
Asteroids	4.5	3	20	0.62	3.2×10^5	1.35×10^4	2.7×10^4
Asteroids	4.5	3.6	20	1.55	1.3×10^4	1.35×10^4	2.7×10^4

We see that when β and B_f are greater than B, more craters can be produced than are observed; $B_f > B$ implies there is obliteration for some of the craters with $D > D_c$. However for $\beta = 4.5$ and $\nu = 3.6$, the number of produced craters approximately equals the number of observed craters; this case cannot account for the additional number of obliterated craters. Such holds generally for all $\beta > 3$ cases of interest. For this reason we employ only the case $\nu = 3$ in the calculations for $\beta > 3$ below. Thus, if there is other evidence that $\beta > 3$, we can derive the interesting conclusion that $\nu \simeq 3$.

We now take account of crater obliteration in comparing the number of craters produced by asteroids with the number actually present at some epoch. Again we assume that the present rate of asteroidal bombardment is representative of the past. Equation (6) with $D_c = 20$ km gives the total number of craters ever produced by asteroids in 4.5×10^9 years. The number of craters produced with diameters greater than D, independent of subsequent obliteration, is also given by

$$\frac{A_f}{(B_f - 1)} D^{-(B_f-1)} ,$$

where $B_f = \beta$ for $\nu = 3$, by equation (8). The value of A_f is obtained by demanding that the number of craters given by this expression with $D = D^*$, the diameter at which obliteration ceases, equals the observed number of craters with diameters in excess of D^*. We finally require that the number of craters larger than 20 km produced by asteroids equal the total number of such craters ever produced, independent of subsequent obliteration (as extractable from the crater counts):

$$\frac{T_{\sigma'}}{t_{\sigma'}}\left[(200)(20)^{\beta-2}\right]\frac{X_c^{-(\beta-1)}}{(\beta - 1)} = \frac{AD^{*(\beta-B)}}{(B - 1)(20)^{\beta-1}} . \qquad (9)$$

The quantity in the brackets is k_1, and X_c is the value of X corresponding to D = 20 km (see equation (5) and Table 4). For the observed frequency relation and a given value of β, we can then solve equation (9) for D^*. The results are given in Table 5.

Table 5. Estimates of D^* from distribution functions

β =		3.5	4.0	4.5	5.0
D^* (km)	eq. (7a)	20	56	95	131
	eq. (7b)	12	68	133	181

We see that for $4.0 \leq \beta \leq 5.0$ we obtain values of D^* consistent with $\beta > B$ and with the earlier estimates of D^*_{min} (Table 3). Values of β larger than 5 would seem outside both theoretical and observed slopes. Thus, asteroids with a bombardment rate similar to the present rate can account for the Martian craters in a consistent manner. In this approach we require the absolute values of the distribution-function exponents for the asteroid distribution and for the craters when first produced to be substantially larger than the observed crater value. We show in Section 6 that for $B_f > 3$, $\alpha = B_f - 3$. Thus, for a uniform bombardment rate, craters are being eroded by a process for which $1 \leq \alpha \leq 2$. This value of α is entirely consistent with known erosional mechanisms, discussed in Section 6. Alternatively, we can follow the suggestion that the bombardment rate was greater in the past and have the two exponents, β and B, agree or at least be closer in value.

5. MAJOR TOPOGRAPHICAL FEATURES AS POSSIBLE CRATERS

Several large Martian bright areas, such as Elysium, Eridania, Hellas, and the Isidis Regio-Neith Regio complex, have a strikingly circular appearance, and it is natural to inquire whether these could be the results of impacts caused by very large asteroids. This view is consistent with several recent studies indicating that the bright areas tend to be lowlands (Sagan and Pollack, 1966b; Sagan et al., 1967). The bright areas of the sort mentioned have a diameter of 1000 km or more and would require an impacting object of diameter approximately 35 km or larger to create them. At present there are five Mars-crossing asteroids with diameters exceeding 35 km. Since the mean collision time with Mars is approximately equal to the lifetime of the planet (Öpik, 1963), the present number of Mars-crossing asteroids is capable of explaining such features without the invocation of a higher bombardment rate in the past. This model is consistent with $\beta > 3$. On the other hand, suppose we accept the suggestion of a very high initial bombardment rate with the exponent β equal to 2.5. Then Table 4 implies that the predicted number of Martian craters must be raised by at least a factor of 20 over the number predicted with a uniform bombardment rate; thus, there should be over 100 craters with diameters exceeding 1000 km. Mars is certainly not saturation bombarded at such a resolution. If any other erosion mechanism were to remove most of the 100 craters with $D > 1000$ km, it would be even more effective for smaller diameters where we should see no craters at all. Therefore, unless we wish to invoke histories that were very different for large asteroids than for small ones, these predictions based on $\beta = 2.5$ seem contrary to observations; for this reason a more uniform bombardment rate with β substantially larger than 2.5 seems to be preferred. Were the dark areas lowlands, the same conclusions would follow, since even fewer very large circular dark areas exist on Mars.

6. EROSION MECHANISMS

In this section we discuss various mechanisms by which newly formed craters can be eroded and obliterated. The damage produced by impacting objects on nearby craters will be the first such process to be considered; we will discuss it rather extensively since it is readily susceptible to a quantitative treatment.

When a sufficient number of craters is produced, the probability becomes large that new craters will form on or near existing craters. If the size of the new crater is comparable to or larger than the old crater, and if the new crater is produced within the same area as the old one, it will clearly tend to obliterate the old crater. If the impacting object falls sufficiently close to, but not contiguous with, the old crater, it may still obliterate the old crater both by filling in the old crater with some of the debris created in the formation of the new crater and by the damage caused by surface shock waves generated by the new impact. Finally, when the old crater is far enough away from the center of the new crater not to be destroyed totally, it may nevertheless be sufficiently close to the new crater to suffer substantial damage. Similarly, new craters small in size compared to an old crater will not be able to destroy the preexisting crater, but they can damage it. Thus, in several ways, impacts are capable of causing erosion and obliteration of craters. In what follows we will try to distinguish carefully between obliteration of craters by subsequent impacts and erosion of craters by a similar mechanism.

We now proceed to examine the extent of the impact damage present for the two cases discussed earlier: $B_f = B$ and $B_f > B$. In the first case, the diameter-frequency relation for the generated craters has the same exponent as the relation for the observed craters, but a large initial bombardment rate is needed to account for the observed number of craters; the second case presumes a constant bombardment rate and a larger exponent for the generated craters.

In assessing the importance of impact damage, we will compute three important variables: the crater number density; the slope, B, of the diameter-frequency relation; and F, the fraction of the total surface area that has been significantly disturbed by impact damage. Initially, we confine the discussion to obliteration by impact, and return later to erosion. When $F \sim 1$, so that impact obliteration is important, there will be an accompanying modification in the crater number density and, in some cases, in the value of B, as compared with values expected in the absence of impact obliteration.

We begin by obtaining an expression for F under the assumption that impact damage is the only important obliteration mechanism. From the previous discussion, $n_f(D)dD$ is the number of craters between D and D + dD that have been produced over the entire Martian surface within the lifetime of the planet. Therefore, $n_f(D)dD/4\pi R_{\sigma}^2$ represents the number of such craters produced per unit area, with R_{σ} as the radius of Mars; $D^2 n_f(D)dD/16R_{\sigma}^2$ is then the fraction of the area of Mars covered by such craters. Finally, if old craters within $\sqrt{\epsilon}(D/2)$ of the center of the impact are obliterated by the formation of a new crater, then $\epsilon\ D^2\ n_f(D)dD/16\ R_{\sigma}^2$ will approximately equal the fraction of the total surface area of Mars that has been significantly disturbed by impact events that form craters with diameters between D and D + dD.

If we integrate over all craters capable of causing obliteration to a crater of size $\tilde{D}$, we obtain

$$F \simeq \frac{\epsilon\ A_f}{16\ R_{\sigma}^2} \int_{D_\ell}^{D_u} D^{-B_f}\ D^2\ dD$$

$$= \begin{cases} \dfrac{\epsilon\ A_f}{16\ R_{\sigma}^2 (3 - B_f)} \left[D_u^{3-B_f} - D_\ell^{3-B_f} \right] \equiv Q, & \text{if } B_f \neq 3 \\ \dfrac{\epsilon A_f}{16\ R_{\sigma}^2} \log_e \dfrac{D_u}{D_\ell} \equiv Q, & \text{if } B_f = 3 \end{cases} \qquad (10)$$

where D_u is the size of the largest crater actually produced, and D_ℓ is the size of the smallest crater that will by itself be effective in obliterating a crater of size $\tilde{D}$. We expect that $D_\ell \simeq \tilde{D}$. Formally, we write $D_\ell = g\tilde{D}$; we can anticipate that $g \simeq \epsilon^{-1/2}$.

Equation (10) implicitly neglects the possibility that two craters may partially share the same area and hence that F will actually be smaller than Q. The correct formula for F when $Q \geq 1$ is given by

$$F = 1 - \exp(-Q) \quad . \tag{11}$$

Note that $F \simeq Q$ when $Q \ll 1$, and that $F \to 1$ as $Q \to \infty$, as should be the case. For $Q > 1$, Q is the mean number of times a given area has been cratered; it is a measure of the generation number of the observed cratering. We next wish to estimate $\overline{\phi}$, the mean fraction of craters of a given diameter that survive to the present epoch. Since we know how to calculate the number of craters that have been produced during the history of the planet, we can readily derive the present observable crater density and thus estimate both A and B.

If a crater is formed at a time, t, in the past, its probability of obliteration, P(t), is given by $1 - \exp[-Q(t)]$, where Q(t) is the appropriate value of Q between time t and the present (t = 0). Thus, the statistical average of the number of craters formed at time t with diameter D that survive to the present, $\phi(t)$, is simply $\exp[-Q(t)]$. The statistical fraction of craters of diameter D, formed at any epoch, that survive until the present epoch, is

$$\overline{\phi} = \frac{\int_{T_\sigma}^{0} \phi(t)\, R(t)\, dt}{\int_{T_\sigma}^{0} R(t)\, dt} \quad , \tag{12}$$

where R(t) is the relative bombardment rate at time t. If we assume R(t) is independent of D, then Q(t) is given by the following time-integration of the bombardment rate:

$$Q(t) = Q(T_{\delta}) \frac{\int_t^0 R(t')\, dt'}{\int_{T_{\delta}}^0 R(t')\, dt'} \quad . \tag{13}$$

If we set $y = \int_t^0 R(t')\, dt'$ and $z = -\, y\, Q(T_{\delta}) \Big/ \int_{T_{\delta}}^0 R(t')\, dt'$, we readily find

$$\overline{\phi} = \frac{1}{Q(T_{\delta})} \left\{ 1 - \exp\left[- Q(T_{\delta}) \right] \right\} \quad . \tag{14}$$

Thus, $\overline{\phi}$ is independent of R(t), as we expect. Also, as $Q(T_{\delta}) \to 0$, then $\overline{\phi} \to 1$; as $Q(T_{\delta}) \to \infty$, so $\overline{\phi} \to 1/Q(T_{\delta})$. A result similar to equation (14) has been obtained by Walker (1967).

In the absence of obliteration, the observed number of craters of diameter D would simply equal the number formed, $n_f(D) = A_f D^{-B_f}$. Obliteration reduces the observed number of craters to an equilibrium number

$$n_e(D) \equiv A D^{-B} = \overline{\phi}\, A_f\, D^{-B_f} \quad , \tag{15}$$

where A and B are the observed values.

When there is a very large number of craters formed, so that $Q \to \infty$, equation (15) reduces to a simpler and explicit dependence on diameter. As $Q \to \infty$, $\overline{\phi} \to 1/Q$. In equation (10), which determines Q, we set $D_{\ell} = \epsilon^{-1/2} D$. If, finally, $D_u >> D_{\ell}$, we obtain a simple expression for $\overline{\phi} = 1/Q$, which, when inserted in equation (15), yields

$$n_e(D) = \frac{16\, R_{\sigma}^2}{\epsilon}(3 - B_f) D_u^{B_f - 3} D^{-B_f}, \quad B_f < 3 \tag{16}$$

$$n_e(D) = \frac{16\, R_{\sigma}^2}{\epsilon}\left[\log_e\left(\frac{D_u}{g\, D}\right)\right]^{-1} D^{-B_f}, \quad B_f = 3 \tag{17}$$

$$n_e(D) = \frac{16\, R_{\sigma}^2}{\epsilon}(B_f - 3) g^{B_f - 3} D^{-3}, \quad B_f > 3 \quad . \tag{18}$$

In the previous section we suggested that craters larger than 1000 km in diameter must be expected occasionally. Thus, for the craters of interest $D_u >> D_\ell$ will always be fulfilled. Since craters with $D > R_{\sigma}$ are not to be expected, we select $D_u \simeq 3000$ km. As equations (16) through (18) indicate, our results will not be very sensitive to the exact choice of D_u, for the acceptable range of B_f values. Similarly, we see from equation (14) that Q need not be very much larger than unity for $\overline{\phi} \simeq 1/Q$ to be a good approximation. Equations (16) through (18) are similar to the ones derived by Marcus (1967) and by Walker (1967) in lunar context.

We now employ the equations derived above to assess the significance of impact obliteration. First we consider the case $B_f = B$, and compute F from equations (10) and (11). If B = 2.5, we see from equation (10) that when $D_\ell << D_u$, the value of F depends almost entirely on the size of the largest crater, D_u. Accordingly, we set $D_\ell = 0$. We let A_f equal the observed value of A and so find a lower limit to F. When B = 3.0, we proceed in a similar fashion. Since Q depends only logarithmically on the choice of D_ℓ, we select D_ℓ = 30 km, and consider the results as representative rather than exact.

In Table 6 are summarized these calculations of F for $B_f = B$ for two choices of ϵ. In each of these cases there will be some obliteration attributable to the cratering process itself. But the extent of obliteration depends sensitively on the degree to which A_f exceeds A, and on the value of ϵ.

Since in all cases the lower limits on F are not very small, some craters have been obliterated; thus, the lower limit on A_f must be somewhat in excess of A. Accordingly, the lower limits on F for the first four entries of Table 6 must be raised somewhat.

Table 6. Predicted values of F

B_f	B	$\sqrt{\epsilon}$	$\tilde{D}$	F
2.5	2.5	1	—	≥ 0.66
2.5	2.5	2	—	≥ 0.96
3.0	3.0	1	—	≥ 0.47
3.0	3.0	2	—	≥ 0.92
4.0	2.5	1	20 km	0.38
4.0	2.5	2	20	0.98
4.0	2.5	1	50	0.17
4.0	2.5	2	50	0.78
4.0	2.5	1	D*	0.16
4.0	2.5	2	D*	0.74
4.5	2.5	1	20 km	0.83
4.5	2.5	2	20	1.00
4.5	2.5	1	50	0.35
4.5	2.5	2	50	0.99
4.5	2.5	1	D*	0.16
4.5	2.5	2	D*	0.85
5.0	2.5	1	20 km	1.00
5.0	2.5	2	20	1.00
5.0	2.5	1	50	0.70
5.0	2.5	2	50	1.00
5.0	2.5	1	D*	0.16
5.0	2.5	2	D*	0.94

We next compare predicted with observed slopes and crater densities, still for the case $B_f = B$ and now for saturation bombardment. For $B_f = 2.5$, equation (16) shows consistency: the slope of the observed crater distribution

exactly equals that of the craters formed with no obliteration. This is almost true for $B_f = 3$ (equation (17)); there is only a slow logarithmic dependence on diameter besides the D^{-3} dependence. This agreement even holds somewhat short of complete saturation bombardment, since $\overline{\phi}$ has little D-dependence for these choices of B_f. It is interesting that when $B_f = B = 2.5$, almost all the obliteration is due to the very largest craters — craters unlikely to be detected on the Mariner 4 photographs.

A comparison of the observed and predicted crater densities is readily made by comparing the observed value of A with the coefficient of D^{-B_f} in equations (16) and (17). Agreement to within 20% is secured for $B_f = 2.5$ with $\sqrt{\epsilon} = 1$, and for $B_f = 3.0$ with $\sqrt{\epsilon} = 1.25$. The predicted values are based on the assumption of complete saturation bombardment. The minimum values of F (first four entries, Table 6) indicate that this assumption is reasonable. If bombardment is actually less than saturation, the predicted values of A are lowered and a smaller value of $\sqrt{\epsilon}$ is required to secure agreement. However, $\sqrt{\epsilon} \geq 1$ should hold always; $\sqrt{\epsilon} = 1$ holds for obliteration only when a crater is formed on area occupied by a preexisting crater. Thus, the observed crater densities are very close to the saturation limit for $B_f = B$.

We next turn to the $B_f > 3$ cases. The parameter F is obtained as before from equations (10) and (11); again, we assume $D_u \gg D_\ell$. However, in this case, we can directly estimate F, rather than find a lower limit. Table 5 displays estimates of D^*. Thus, A_f can be obtained by demanding that the number of craters with $D > D^*$ equal the observed value. When $B_f > 3$, equation (10) implies that the smallest craters capable of causing obliteration make the principal contribution to F. Accordingly, we set $D_u = \infty$ in equation (10) with little loss of accuracy. For crater formation to be an important obliteration mechanism, several constraints on F must be met. The values of D^* in Table 5 refer to diameters at which obliteration is just becoming important; roughly, $F(D^*) \sim 0.1$. Also, F should lie close to unity for the smaller craters. We see from Table 6 that these requirements are met for appropriate choices of $\sqrt{\epsilon}$.

According to equation (18), the predicted slope will be -3 at saturation, independent of the value of B_f. The predicted slope is then again in good agreement with the observations. On the other hand, if there is substantially less than saturation bombardment, the predicted slope will be closer to B_f and so will disagree with the observations. Such a disagreement would indicate that impact damage is not the major cause of crater obliteration. To secure sufficient agreement with observation, we require that Q be large enough that the effective slope be within 10% of the saturation value for 25 km $\leq D \leq$ 50 km. (The observed slope is heavily influenced by the smaller craters, which are the most numerous.) This demand implies that $F(D = 50 \text{ km}) \gtrsim 0.75$. This, coupled with our previous requirement that $F(D^*) \sim 0.1$, can be used to test the results. The restriction that the slope be close to the saturation value implies that the number of observed craters should be close to the saturation limit.

Table 6 exhibits the values of F at D = 20 km, 50 km, and D^*, and for various choices of B_f and ϵ. In all these $B_f > B$ cases, B = 2.5 was adopted, but essentially identical results obtain for B = 3.0. We see that for $B_f = 4.5$ and 5.0 the two constraints on F can be satisfied for appropriate choices of ϵ. For $B_f = 4.0$ the two constraints cannot simultaneously be satisfied, since D^* is only slightly larger than 50 km (cf. Table 5). However, for such a value of B_f, less variation in B_f is required to obtain the observed value of B than is the case for larger B_f; and even the $B_f = 4$ case may not be incompatible with the data.

We next compare, by equation (18), the observed number of craters with the number predicted for $B_f > B$ and saturation bombardment. If B = 3, we can directly compare the observed value of A with that predicted from equation (18). The two results agree when $\sqrt{\epsilon}$ is slightly larger than 2. (Actually, a somewhat smaller value of $\sqrt{\epsilon}$ is implied, because the predicted crater density is slightly overestimated.) Since the observed value of A depends on the curve-fitting decision B = 2.5, we cannot directly compare the predicted and observed values of A when B = 2.5. Rather, we compare the observed number of craters between 20 km and D^* with the predicted numbers, by integrating equation (18) between 20 km and D^*. Table 7 shows the results of such a calculation for various values of B_f and $\sqrt{\epsilon}$. Again

noting that the predicted values are slight overestimates, we see that the model can agree with the observations when the radius of the zone of obliteration, $\sqrt{\epsilon}(D/2)$, is about twice the size of the crater produced by the object causing the obliteration. For this B_f range, $n_e(D)$ is proportional to a power of ϵ between -1.5 and -2.

Table 7. Predicted and observed number of craters on Mars, $20 \text{ km} \leq D \leq D^*$, $B_f > 3$

B_f	$\sqrt{\epsilon} = 1$	$\sqrt{\epsilon} = 2$	$\sqrt{\epsilon} = 3$	Observed value
4	2.0×10^5	2.5×10^4	7.4×10^3	1.1×10^4
4.5	3.3×10^5	2.9×10^4	6.9×10^3	1.2×10^4
5	4.4×10^5	3.0×10^4	6.1×10^3	1.3×10^4

We conclude that, for all categories of B_f, impact damage may contribute significantly to crater obliteration, yielding values of $F \sim 1$. All models seem capable of accounting for the observed number of craters as well as for the exponent of the diameter-frequency relationship. It is quite noteworthy that the observations are of so little use in distinguishing among the hypotheses in the case of near-saturation bombardment. Future photographic missions with better resolution (increasing the usable range in D before incompleteness sets in) or better areal coverage (decreasing the probable errors in A and, especially, B) might permit a useful distinction among the models. It would also be useful to establish more rigid constraints on the value of $\sqrt{\epsilon}$, to better determine the importance of impact damage.

The influence of impact damage on crater <u>erosion</u> can be estimated by calculating F for erosion from equations (10) and (11). We must employ a larger value of ϵ than that used for obliteration. Thus, F for erosion will be larger than F for obliteration. We see from Table 6 that crater impact should contribute significantly to the erosion of craters when $B_f = B$, and for most circumstances where $B_f > B$.

It is relatively easy to visualize the effects of erosion of craters for the $B_f > 3$ case. Chapman (1968) has argued that, in a small-scale lunar context, the effect of erosion with large B_f is to soften all old topographical features on a scale approximating the depths of craters that saturate the surface (for $\sqrt{\epsilon} = 1$). That is, the scale of softening approximates $D_\ell/10$ for D_ℓ such that $Q \sim 1$. For cases where $\sqrt{\epsilon} > 1$, the scale of softening is probably about $\sqrt{\epsilon}\,(D_\ell/10)$ for D_ℓ such that $Q \sim 1$. Nearly all craters of sizes smaller than the appropriate D_ℓ will be soft, crater-like depressions with no sharp features. The percentage of fresh Class 1 craters will be very small, smallest for higher B_f's (less than 1% Class 1 for $B_f = 4.5$). For $\sqrt{\epsilon} = 1$, the scale of softening is only about 0.5 to 3 km — probably too small to be noticeable on the Mariner photographs. For $\sqrt{\epsilon} \sim 2$, we might expect to see the softening of the older features on a scale of about 1 to 6 km for $B_f = 4.0$ and 5.0, respectively. This is again probably below the resolution of the Mariner photographs, and the walls of the older craters do not generally appear substantially softened. It is possible that such a large-B_f saturation-cratering process could create sufficient dust to give the craters their characteristic filled-in appearance, provided the created dust was adequately mobile (see Section 7).

We now summarize the results of impact on crater obliteration and erosion. In all cases, impacts will cause some obliteration; the question at issue is whether this is the dominant process. We have found that the observed crater densities are close to or equal to saturation values for $B_f = B \simeq 3$; impact obliteration is clearly dominant for this case. However, the question cannot properly be answered for the $B_f > B$ case, because of our lack of precise knowledge on the value of $\sqrt{\epsilon}$ for Mars. In this case, the principal obliterating craters are comparable in diameter to the craters being obliterated; such circumstances exist on the Moon, where similarly sized craters overlap one another, both remaining visible. For the Moon, then, $\sqrt{\epsilon}$ is probably not much above 1.0. If such a value applied to Mars as

well, a contradiction would exist with the $\sqrt{\epsilon} \simeq 2$ requirement for $B_f > B$ (Table 6), and we would conclude that saturation bombardment is not the dominant obliteration mechanism for $B_f > B$. However, for all we know, Martian and lunar soil conditions differ sufficiently to permit $\sqrt{\epsilon} \simeq 2$ for Mars. It is also possible that some incompleteness exists in the crater counts even for $D > 20$ km, in which case the required $\sqrt{\epsilon}$ would be lowered. In all cases, impact damage is a contributing factor in crater erosion. The value of the obliteration parameter, a, may be obtained directly from equations (16) through (18):

$$a = B_f - B \quad . \tag{19}$$

Thus for the low B_f values, $a \simeq 0$, while for the high B_f values, $1 \leq a \leq 2.5$.

We now briefly mention other possible agents of crater erosion and obliteration. There is good evidence that dust abounds on Mars and that this dust is moved about by winds (see, e. g., Sagan and Pollack, 1967). Since the present winds can lift up dust, and since aeolian erosion and filling by dust must be occurring today, we can make no inferences about the possibility of a much larger atmosphere in the past, contrary to a conclusion of Leighton et al. (1965). Indeed, the limiting factor on the effectiveness of dust as an erosional agent is the very large quantities of dust needed to fill a significant portion of most of the observed craters and to fill completely whatever craters have been obliterated; the average depths of the observed craters is several kilometers. We show in the next section that an amount of fractured material approaching this figure has been produced during cratering. If the dust is very friable, much of it will eventually have been converted into particles with sizes < 200 μ, as are required for saltation, suspension, and dispersal by momentum exchange (cf. Sagan and Pollack, 1967). It is also possible that accretion of interplanetary dust may play a

role. The present accretion rate on the Earth is uncertain, but apparently lies between 2×10^{-14} and 2×10^{-16} g cm^{-2} sec^{-1} (Parkin and Tilles, 1967). If this dust is primarily of asteroidal origin, we expect an influx rate ~ 20 times greater on Mars than on the Earth. For dust of low density, this leads to thicknesses ranging from a few meters to a fraction of a kilometer. Filling and aeolian erosion involving dust may be particularly important for erosion of smaller craters with depths < 1 km. The preponderance on Mars of flat-floored craters with a filled-in appearance, compared with highly battered craters with misshapen walls in the lunar highlands, suggests that filling by dust or lava is likely to be a more important erosive agent on Mars than on the Moon.

It is difficult to examine these filling processes quantitatively. Nevertheless, a brief consideration of an idealized dust-filling model will demonstrate the compatibility of filling processes with the observed distribution of Martian craters by class. Consider the crater profile shown in Figure 8; it is typical of Class 1 lunar craters with diameters about 30 km. The horizontal lines show the crater filled to 15%, 35%, 70%, and 95% of its depth. It is our opinion that these percentages approximately represent the divisions between the four classes (e. g., craters filled to 15% or less would be classified as 1, those filled to over 95% would not be recognized as craters at all). What follows does not depend strongly on the precise percentages chosen.

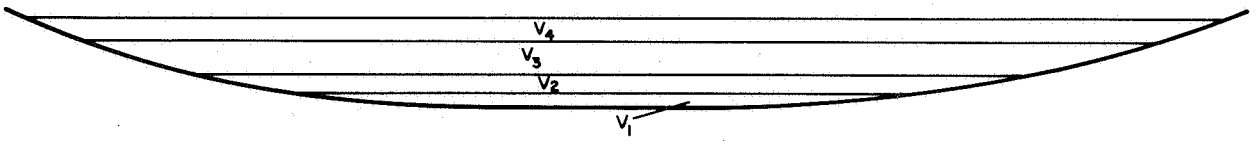

Figure 8. Influence of filling by dust or lava on the class membership of a crater.

For a model in which mobile dust (or fluid) is uniformly deposited over the surface of Mars, craters will collect dust at a rate proportional to D^2. But since the crater volume scales as D^3 (assuming that the same profile and depth-diameter ratio holds for all diameters), the crater lifetime will scale as D (hence $\alpha = 1$). Baldwin's (1963) Figure 20 suggests that for his Class 1 lunar craters, the diameter-depth ratio is not constant but that the depth varies as $D^{0.6}$. Presumably the fact that larger craters are proportionately more shallow than smaller ones is due either to the details of the process of crater formation, or to rapid isostatic adjustment of the larger craters following their formation. In this case, $\alpha = 0.6$ for filling such craters with dust.

In either case, for a crater of a given diameter, the relative lengths of time the crater spends in each class will equal the relative volumes of the four slabs shown in Figure 8. Therefore, as discussed in Section 3, the relative volumes of the four slabs should equal the relative numbers of craters in each class, for the dust-filling model. The volumes for the slabs of the crater shown in Figure 8 are presented in Table 8, along with the observed percentages of Martian craters in each class. The agreement of the model with the observations is good.

Table 8. Percentages of craters by class

Class	Dust-filling model	Observation (D > 20 km), N = 53
1	4	4
2	12	9
3	43	40
4	41	47

Another conceivable mechanism of surface erosion is the laying down of sediment within the crater through the intermediation of running water or of occasional flash floods. Water erosion seems to be a major cause of the obliteration of terrestrial craters. Hartmann (1966) has compiled data on

craters in the geologically stable Canadian Shield region, and his results imply that in this area only craters larger than about 50 km are capable of surviving for several billion years. The Canadian Shield region has probably not been periodically submerged under water, as, say, the Mississippi Basin has, and so has been eroded primarily by running water and by glaciers. Hartmann's data imply $\alpha \simeq 2$ for these water-dependent terrestrial erosion mechanisms.

The value of D^* deduced for the Canadian Shield is quite comparable to the value deduced here for Mars. Thus, as far as erosion rates are concerned, there is nothing in the Mariner 4 photographs that excludes running water or glaciers on Mars until quite close to the present epoch. It has been stated that none of the characteristic geomorphology of running water (e.g., the dendritic patterns of river basins) is visible on the Mariner 4 photographs; but very suggestive signs of some variety of fluid flow do appear, e.g., on Picture 11. It has also been argued (Sagan, Levinthal, and Lederberg, 1968) that liquid water may be available on contemporary Mars — generally, in grain interstices and subsurface microenvironments for a fraction of an hour each day, and, more rarely, on a much larger scale. Even if liquid water is present only in such isolated times and places, its contribution to erosion over several billion years may be very great. In addition to the contribution of running water, the volume changes of water during freeze-thaw cycling on Mars can be a very potent erosive agent.

Mountain building on the Earth, on a scale needed to obliterate a crater 100 km across and several kilometers deep, seems to occur on a time scale similar to the age of the Earth. Thus, the presence of long-lived, large Martian craters places no severe constraints on such mountain-building activity on Mars. The 0.5% of the Martian surface viewed by Mariner 4 displayed no obvious folded mountain chains. On the other hand, the existence of major elevation differences (Sagan et al., 1967; Sagan and Pollack, 1966b) involving noncircular regions and the probable presence of ridges resembling terrestrial tectonic dikes (Sagan and Pollack, 1966a) seem to argue that diastrophism may be another cause of erosion on Mars. Unfortunately, we have no

ready way of examining such possibilities in greater detail at present; it would be interesting to investigate the extent to which particular erosion mechanisms lead to distinctive crater morphologies on Mars.

We have seen that several erosion mechanisms lead to $2.0 \geq a \geq 0.6$. For uniform bombardment, we have found independently in Sections 4 and 6 evidence that $2.5 \geq a \geq 1$; and evidence in Section 5 indicated that fairly uniform bombardment has in fact occurred.

In summary of this section, crater overlap and near-saturation bombardment as a mechanism for crater erosion and obliteration are susceptible to quantitative treatment and seem able to account for much of the damage sustained by the Martian craters. Erosion due to windblown dust of impact or of micrometeoritic origin, liquid water on large or microscales, mountain building, and flooding by lava cannot be excluded within present knowledge as possible contributing mechanisms to crater erosion during the history of Mars.

7. CRATERS AS SOURCES OF DUST

Polarimetric, photometric, and infrared radiometric studies have shown the Martian surface is covered with dust (cf. Pollack and Sagan, 1967). Radar observations of the bright areas indicate that the dust extends down to a depth of at least a meter (Sagan and Pollack, 1965). One abundant source of such a large amount of dust is the cratering process; the hypervelocity impacts responsible for the craters pulverize and eject large amounts of material.

We now estimate the average depth to which the currently observed craters have penetrated the Martian surface. As before, $A\, D^{-B} D^2 / 16\, R_{\sigma}^2$ equals the fraction of the surface covered by these craters. The average depth, $\langle S \rangle$, to which the Martian surface has been penetrated by craters with diameters from D_ℓ to D_u is then given by:

$$\langle S \rangle = \frac{A}{16\, R_{\sigma}^2} \int_{D_\ell}^{D_u} S\, D^{-B+2}\, dD$$

$$= \frac{A\, h}{16\, R_{\sigma}^2 (4 - B)} \left(D_u^{4-B} - D_\ell^{4-B} \right) \quad , \tag{20}$$

where we have assumed $S = h\, D$; h is approximately 1/20 for the craters of interest.

For $B < 4$, $\langle S \rangle$ depends mostly on D_u. For $B = 2.5$, and D_u chosen between 100 and 1000 km, $\langle S \rangle$ ranges between a few hundred meters and > 1 km. When the obliterated craters are taken into account, $\langle S \rangle$ will be somewhat raised. For the larger craters, $S = hD$ applies instantaneously at impact, but isostatic adjustment may rapidly make such craters quite shallow. Thus, the very largest impact craters may have the entertaining property of producing much more ejecta than is required to fill them entirely — the surplus will fill smaller craters that are not isostatically compensated. On the other hand, when $B > 4$, $\langle S \rangle$ depends mostly on D_ℓ, and the largest craters tend not to play a major role in producing ejecta. But here again, reasonable choices of D_ℓ yield values of $\langle S \rangle$ between 0.1 km and several kilometers. In either case, ejecta produced by impact could make major contributions to crater erosion. If even a very small fraction of the ejecta so produced is eventually converted into particles small enough to be moved by contemporary Martian winds, it will have a large enough volume to cover the bright areas to a depth of a meter, which is the lower limit placed by the radar observations. The cratering process is, therefore, a promising mechanism to account for the large quantities of dust present on Mars.

8. CRATER AGES

Much of the previous analysis of the Mariner 4 cratering statistics has been devoted to a determination of the "age" of the Martian surface; i.e., the time since the underlying features have been eroded away (Leighton et al., 1965; Anders and Arnold, 1965; Baldwin, 1965; Witting et al., 1965; Öpik, 1965, 1966; Binder, 1966; Hartmann, 1966). These authors have generally made a comparison of the crater densities in the Mariner 4 region of Mars with those of the lunar maria. The age of the Martian surface then depends on an estimate of the relative bombardment rates, and a guess of the age of the lunar maria. With the maria assumed to be several billion years old, the Martian surface has been estimated to have ages ranging between 0.8×10^9 and 4.5×10^9 years. An obvious uncertainty in this procedure is the estimate of the age of the lunar maria.

Within the context of the models of the present paper, we can obtain ages directly from the Martian crater counts, and independently of the age of the lunar maria. Such a procedure ultimately depends on estimates of the absolute bombardment rate on Mars. Models with $\beta < 3$ require, as we have shown, a great flurry of crater formation in the early history of the planet; thus, almost all cratered areas would have an age comparable to that of Mars. For those models with $\beta > 3$, a more uniform bombardment rate is implied; the largest craters, with $D > D^*$, will again have an age comparable to that of Mars, but the mean age of such craters will be half the age of Mars. As Hartmann (1966) has quite properly emphasized, the ages of craters with $D < D^*$ will be a function of D. A unique crater age for the Martian surface is an erroneous concept for $\beta > 3$.

For $D < D^*$, we note that the crater age is given by $N_e(D)/\tau = n_f(D)/T_0$. Since $n_e(D) \propto D^{-2.5}$, by observation (equation 7a), and $n_f(D) \propto D^{-\beta}$, by hypothesis,

$$\tau(D) = \tau(D > D^*)\,(D/D^*)^{\beta - 2.5} \quad . \tag{21}$$

We now use equation (22) to calculate $\tau(D)$ for various values of D and β. For a given value of β, D^* was obtained from Table 5. These calculations are summarized in Table 9; also shown are the analogous results obtained using equation (7b).

Table 9. Mean ages of Martian craters (in units of billions of years)

	Diameter, D (km)					
	β	20	40	75	100	500
$B_f = B$	2.5 or 3.0	4.5	4.5	4.5	4.5	4.5
$B_f > B$ equation (7a)	4.0	0.46	1.28	2.25	2.25	2.25
	4.5	0.094	0.64	1.32	2.25	2.25
	5.0	0.022	0.13	0.60	1.24	2.25
$B_f > B$ equation (7b)	4.0	0.66	1.32	2.25	2.25	2.25
	4.5	0.13	0.37	0.95	1.46	2.25
	5.0	0.028	0.11	0.39	0.69	2.25

For the larger craters, the ages are compatible with those derived from assumptions on the ages of lunar maria. For smaller craters (D = 10 - 25 km) and a uniform bombardment rate ($\beta > 3$), the crater ages are tens to hundreds of millions of years; and for still smaller craters the ages are even less. Thus, Martian surface features with dimensions of 10 km or less will, for $\beta > 3$, have ages much less than the age of the solar system. Accordingly, if substantial aqueous-erosion features — such as river valleys — were produced during earlier epochs on Mars, we should not expect any trace of them to be visible on the Mariner 4 photographs unless they were of greater extent than typical comparable features on Earth. Even if $\beta < 3$, the same conclusion follows, because the dust produced by all causes during the subsequent history of the planet should easily be enough to fill such features (cf. Sections 6 and 7). Thus, any conclusion from the Mariner 4 photography that the apparent absence of clear signs of aqueous erosion excludes running water during the entire history of Mars, and makes the origin of life on primitive Mars unlikely, must certainly be regarded as fallacious.

9. VARIATION OF CRATER DENSITIES WITH POSITION ON MARS

In Figure 9, an attempt has been made to localize the positions of Pictures 7 through 14 on the Martian surface. The positions of Martian features are based primarily on a map of the Mariner 4 encounter area drawn by Dr. J. Focas in July 1965, and kindly made available to us through the courtesy of Dr. Focas and of the Meudon Planetary Documentation Center. However, since the combined error of the position of the Mariner 4 frames and of the Martian cartography amounts to at least several degrees in both latitude and longitude, the figure can indicate general correlations only. Any attempt to localize rigorously such a feature as a thin Martian "canal," observed from Earth, on the Mariner 4 photographs, must be doomed to failure. The dashed line indicates the probable outer limits to the position of Mare Sirenum and adjacent dark areas. It is of interest that, within the probable errors of position, Crater 217, the very large crater of Picture 11, is so oriented that its western ramparts vanish just at the boundary between Mare Sirenum and the adjacent semitone area. This is consistent with the hypothesis that the crater was formed on a slope and was subsequently invaded by dust or lava from the brighter lowlands. The crater's resemblance to pre-mare craters on the borders of Mare Humorum is striking; Baldwin (1963, pp. 305-307) has proposed a similar explanation for these lunar craters. Thus, Crater 217 provides some further evidence that dark areas tend to be highlands on Mars.

Crater counts as a function of frame number are shown in Figure 10. The solid dots represent the numbers of all cataloged craters per picture. The open circles represent the same numbers normalized to 10^5 km^2. The crosses represent the number of craters per picture of Quality A and B and of diameter $D > 20$ km. Because of the uncertainties of Quality C statistics, and the incompleteness for $D < 20$ km, it is only the curve connecting the crosses that is significant.

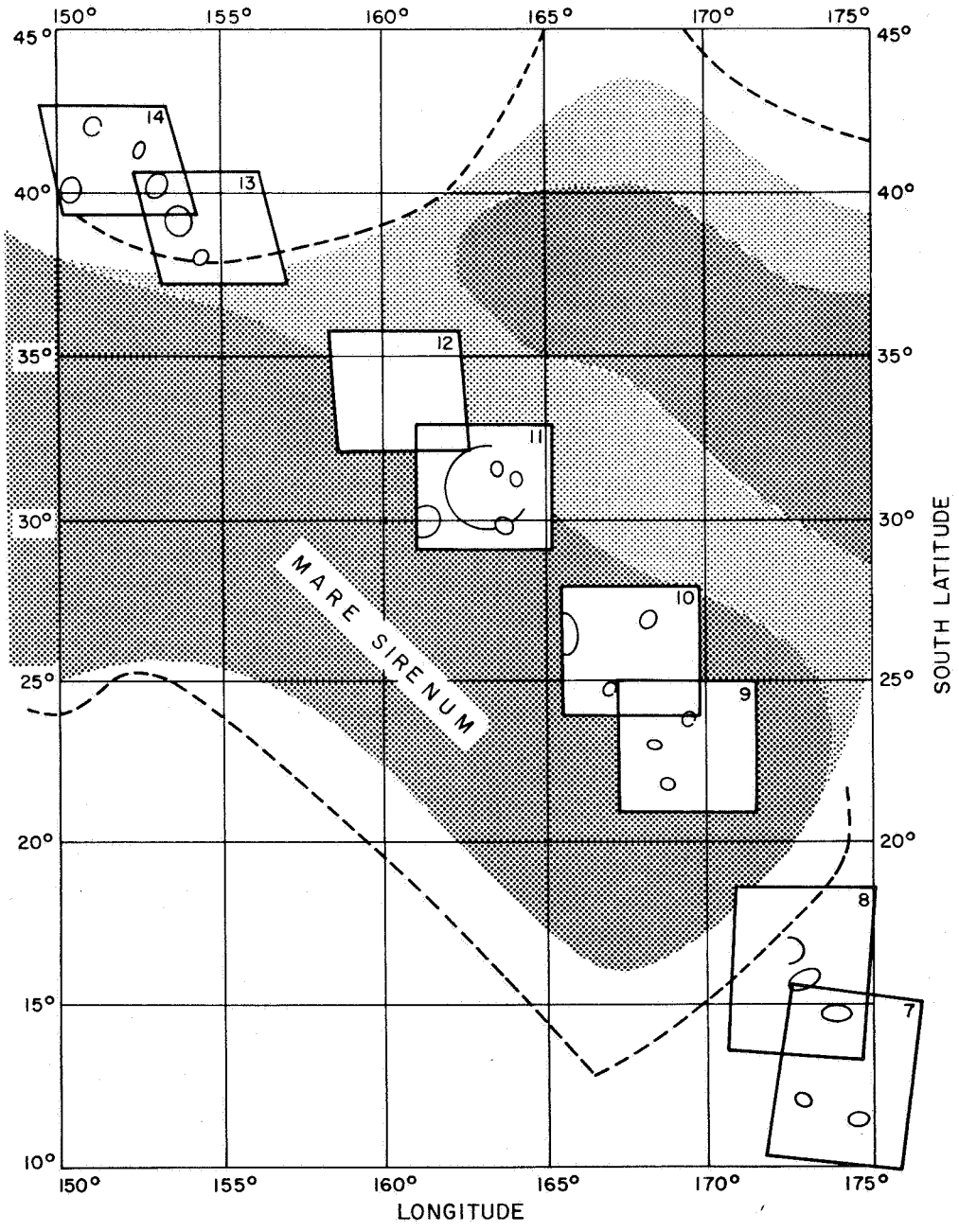

Figure 9. An attempt to localize approximately the positions of Pictures 7 through 14 and their largest craters on the Martian surface. The schematic map is based upon a map drawn by Dr. J Focas at approximately the time of the Mariner 4 encounter. The dashed line indicates the outer limits of the possible positions of the dark areas in the figure.

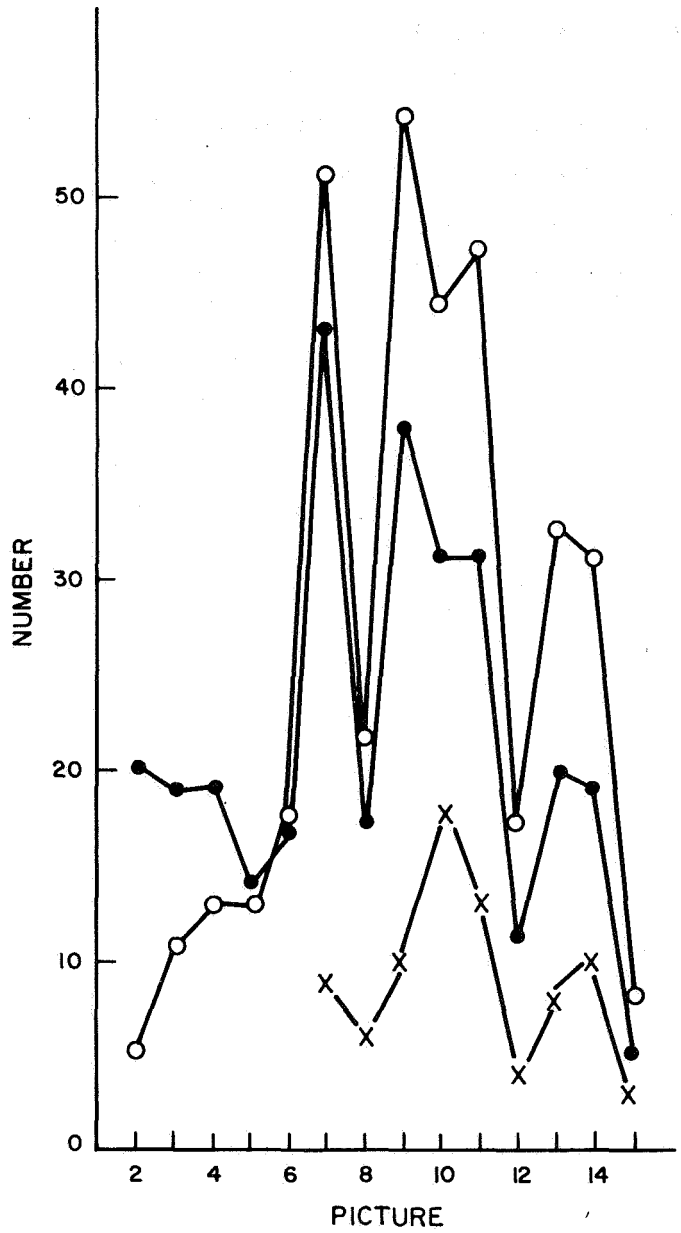

Figure 10. The variation of crater number density with frame number. The dots represent the numbers of all catalog craters per frame; the open circles represent the same numbers normalized to 10^5 km^2; the crosses represent the numbers of craters per frame of Quality A and B, and of diameter larger than 20 km.

Comparing Figures 9 and 10, we see that the highest crater counts, in Pictures 9, 10, and 11, correspond to the only three frames lying entirely or mostly in Mare Sirenum. The adjacent frames of lower crater density — Pictures 7 and 8, and 12 and 13 — lie principally in nearby bright or semitone areas. Thus, a correlation of frames localized in dark areas with frames of high crater density is apparently indicated. However, the crater density in Picture 9, lying entirely in a dark area, is close to that of Picture 14, lying entirely in a bright area. In addition, early Mariner 4 pictures were characterized by high sun, late pictures by a still incompletely understood obscuration. The apparent peak in crater density at Pictures 9 through 11 may, therefore, be nothing more than the convolution of these two effects. If, however, the residual correlation of high crater density with dark areas is real, it indicates a more rapid erosion rate in bright areas than in dark areas. This would be consistent with windblown and drifting dust as an agent of erosion and filling, if the bright areas tend to be lowlands.

10. RECOMMENDATIONS FOR FUTURE WORK

From the conclusions and uncertainties of the present paper, it is clear that there is much room for further work in this subject. Laboratory and field work on the dependence of ϵ on soil type and on the dependence of incompleteness estimates on crater class is needed. Future space-vehicle missions could profitably photograph larger areas to obtain data on the largest craters, to search for relatively uncommon geological features on Mars, and to improve the cratering statistics with better resolution (to narrow the error in B — now hovering precipitously around the theoretically significant value of 3.0), and with a favorable range of solar zenith angles. A close flyby would of course be very useful in this regard, but an orbiter is what is really needed.

ACKNOWLEDGMENTS

We are indebted to Dr. James Edson for high-quality transparencies of the Mariner 4 digital-to-analog data reduction; to Mr. Charles Hanson for preparing photographically contrast-enhanced transparencies of these data; to Drs. J. Focas and A. Dollfus for maps of the Mariner 4 encounter area drawn near encounter; and to Drs. E. Anders, G. Hawkins, G. P. Kuiper, R. B. Leighton, B. C. Murry, R. P. Sharp, and F. L. Whipple for helpful conversations. We are also grateful to Dr. Leighton for permitting us to examine an advance copy of the experimenters' final report (Leighton et al., 1967).

REFERENCES

ANDERS, E. and ARNOLD, J. R.

1965. Age of craters on Mars. Science, vol. 149, pp. 1494-1496.

ARNOLD, J. R.

1965. The origin of meteorites as small bodies. III. General considerations. Astrophys. Journ., vol. 141, pp. 1548-1556.

ARTHUR, D. W. G., AGNIERAY, A. P., HORVATH, R. A., WOOD, C. A. and CHAPMAN, C. R.

1963. The system of lunar craters, quadrant I. Comm. Lunar Planet. Lab., vol. 2, no. 30, pp. 71-78.

1964. The system of lunar craters, quadrant II. Comm. Lunar Planet. Lab., vol. 3, no. 40, pp. 1-2.

ARTHUR, D. W. G., AGNIERAY, A. P., PELLICORI, R. H., WOOD, C. A. and WELLER, T.

1965. The system of lunar craters, quadrant III. Comm. Lunar Planet. Lab., vol. 3, no. 50, pp. 61-62.

ARTHUR, D. W. G., PELLICORI, R. H. and WOOD, C. A.

1966. The system of lunar craters, quadrant IV. Comm. Lunar Planet. Lab., vol. 5, no. 70.

BALDWIN, R. B.

1963. The Measure of the Moon. University of Chicago Press, Chicago, 488 pp.

1965. Mars: An estimate of the age of its surface. Science, vol. 149, pp. 1498-1499.

BINDER, A. D.

1966. Mariner IV: Analysis of preliminary photographs. Science, vol. 152, pp. 1053-1055.

CHAPMAN, C. R.

1968. Interpretation of the diameter-frequency relation for lunar craters photographed by Rangers VII, VIII, and IX. Icarus, in press.

CHAPMAN, C. R. and HAEFNER, R. R.

1967. A critique of methods for analysis of the diameter-frequency relation for craters with special application to the Moon. Journ. Geophys. Res., vol. 72, pp. 549-557.

GAUDIN, A.

1944. Principles of Mineral Dressing. McGraw-Hill, New York, pp.

HARTMANN, W. K.

1965. Terrestrial and lunar flux of large meteorites in the last two billion years. Icarus, vol. 4, pp. 157-165.

1966. Martian cratering. Icarus, vol. 5, pp. 565-576.

HAWKINS, G.

1960. Asteroidal fragments. Astron. Journ., vol. 65, pp. 318-322.

KUIPER, G. P.

1954. On the origin of the lunar surface features. Proc. Nat. Acad. Sci., vol. 40, pp. 1096-1112.

1959. Vistas in Astronautics, Vol. II, edited by M. Alperin and H. F. Gregory. Pergamon Press, New York, p. 273.

KUIPER, G. P., FUGITA, Y., GEHRELS, T., GROENEVELD, I., KENT, J., VAN BIESBROECK, G. and VAN HOUTEN, C. J.

1958. Survey of asteroids. Astrophys. Journ. Suppl., vol. III, pp. 289-428.

LEIGHTON, R. B.

1967. Talk presented at 13th General Assembly, IAU, Prague.

LEIGHTON, R. B., MURRAY, B. C., SHARP, R. P., ALLEN, J. D. and SLOAN, R. K.

1965. Mariner IV photography of Mars: initial results. Science, vol. 149, pp. 627-630.

1967. Mariner ♂ 1964 Project Report: Television Experiment. Part I. Investigators' Report. JPL Tech. Rept. 32-884.

LEVIN, B. J.

1963. The modern form of the impact hypothesis of lunar relief formation. Proc. 13th Intl. Astronaut. Cong., Varna, Bulgaria, Springer-Verlag.

MARCUS, A. H.

1967. Further interpretations of crater depth statistics and lunar history. Letter to the Editor, Icarus, vol. 7, pp. 407-409.

ÖPIK, E. J.

1960. The lunar surface as an impact counter. Mon. Not. Roy. Astron. Soc., vol. 120, pp. 404-411.

1963. Stray bodies in the solar system. Part I. Survival of cometary nucleii and asteroids. Adv. Astron. Astrophys., vol. 2, pp. 219-262.

1965. Mariner IV and craters on Mars. Irish Astron. Journ., vol. 7, pp. 92-104.

1966. The Martian surface. Science, vol. 153, pp. 255-265.

PARKIN, D. W. and TILLES, D.

1967. Influx measurements of extraterrestrial material. Smithsonian Astrophys. Obs. preprint, 40 pp.

POLLACK, J. B. and SAGAN, C.

1967. An analysis of Martian photometry and polarimetry. Smithsonian Astrophys. Obs. Spec. Rep. No. 258, 95 pp.

SAGAN, C., LEVINTHAL, E. and LEDERBERG, J.

1968. Contamination of Mars. Science, in press.

SAGAN, C. and POLLACK, J. B.

1965. Radio evidence on the structure and composition of the Martian surface. Journ. Res. Nat. Bur. Standards, Section D, Radio Science, vol. 69D, p. 629.

1966a. On the nature of the canals of Mars. Nature, vol. 212, p. 117.

1966b. Elevation differences on Mars. Smithsonian Astrophys. Obs. Spec. Rep. No. 224, 45 pp; also in Journ. Geophys. Res. in press, 1968.

1967. A windblown dust model of Martian surface features and seasonal changes. Smithsonian Astrophys. Obs. Spec. Rep. No. 255, 44 pp.

SAGAN, C., POLLACK, J. B. and GOLDSTEIN, R. M.

1967. Radar doppler spectroscopy of Mars: I. Elevation differences between bright and dark areas. Smithsonian Astrophys. Obs. Spec. Rep. No. 221, 75 pp; also in Astron. Journ., vol. 72, pp. 20-34, 1967.

SHOEMAKER, E. M., HACKMAN R. J. and EGGLETON, R. E.

1961. Interplanetary Correlation of Geologic Time. U. S. Dept. Interior, Geological Survey, April.

UREY, H. C.

1962. Origin and history of the moon. In Physics and Astronomy of the Moon, edited by Z. Kopal, Academic Press, New York, chapter 13, pp. 481-523.

WALKER, E. H.

1967. Statistics of impact crater accumulation on the lunar surface exposed to a distribution of impacting bodies. Icarus, vol. 7, pp. 233-242.

WETHERILL, G. W.

1967. Collisions in the asteroid belt. Journ. Geophys. Res., vol. 72, pp. 2429-2444.

WITTING, J., NARIN, F. and STONE, C. A.

1965. Mars: age of its craters. Science, vol. 149, pp. 1496-1498.

YOUNG, J.

1940. A statistical investigation of the diameters and distribution of lunar craters. Journ. Brit. Astron. Assoc., vol. 50, pp. 309-326.

APPENDIX A

CRATER CATALOG FOR MARS FROM MARINER 4 FRAMES 2 THROUGH 6

APPENDIX A

CRATER CATALOG FOR MARS FROM MARINER 4 FRAMES 2-6

Crater number	Frame(s)	Position (cm) from south	Position (cm) from west	Diameter (km)	Class	Quality
1	2	2.8	2.0	35	-	C
2	2	6.2	5.2	42	2	B
3	2	3.0	10.9	28	1	A
4	2	1.4	11.8	17	2	A
5	2	2.9	12.2	39	1	A
6	2	4.9	11.0	73	3	C
7	2	5.0	12.7	51	-	B
8	2	5.2	13.9	70	-	C
9	2	4.9	13.7	21	-	C
10	2	12.5	2.0	38	-	C
11	2	14.2	4.3	70	-	C
12	2	11.2	5.2	87	-	C
13	2	10.0	5.6	31	-	C
14	2	14.2	6.8	36	-	C
15	2	12.9	7.6	94	-	B
16	2	15.0	7.8	42	-	B
17	2	13.8	10.1	21	1	B
18	2	10.4	11.3	86	-	C
19	2	8.7	11.7	63	-	C
20	2	12.6	13.0	18	1	B
21	3,4	3.5,11.6	9.2, 5.9	19,22	-	C
22	3,4	1.0, 8.3	11.1, 7.6	10,12	1	C
23	3,4	6.3,14.2	12.7,10.8	54,46	-	C,B
24	3	6.9	3.0	155	4	C
25	3	10.5	1.9	46	-	B
26	3	11.0	2.8	19	-	C
27	3	9.6	3.3	23	-	C
28	3	12.5	3.1	17	-	C
29	3	11.6	3.5	11	1	B
30	3	11.8	4.0	10	-	C
31	3	11.4	4.1	13	-	B
32	3	10.7	4.3	23	1	A
33	3	9.7	4.1	13	1	A
34	3	9.5	5.5	29	-	C
35	3	8.7	6.3	30	-	C
36	3	10.7	5.5	16	2	B
37	3	11.5	5.9	25	-	B
38	3	14.7	5.5	100	-	C
39	3	11.1	9.2	30	1	A
40	4	1.9	7.8	12	-	C

APPENDIX A (Cont.)

Crater number	Frame(s)	Position (cm) from south	Position (cm) from west	Diameter (km)	Class	Quality
41	4	2.5	10.4	21	-	B
42	4	2.7	11.1	40	2	B
43	4	7.4	6.3	226	-	C
44	4	5.4	11.0	13	1	A
45	4	5.8	11.2	15	1	B
46	4	12.6	1.3	24	3	C
47	4	13.3	5.4	46	-	B
48	4	15.0	6.3	15	-	C
49	4	14.8	7.5	32	-	B
50	4	12.7	8.0	95	-	C
51	4	12.5	9.8	30	2	A
52	4	10.2	11.7	55	-	B
53	4	14.2	13.5	14	-	C
54	4	11.1	12.8	16	-	C
55	4	9.3	14.6	13	-	B
56	5	3.1	6.4	14	-	B
57	5,6	3.5, 12.3	9.9, 2.6	53, 55	3	B, C
58	5,6	4.2, 12.8	13.1, 6.0	54, 52	-	C
59	5,6	4.0, 12.8	14.7, 8.2	12, 12	-	C
60	5	9.6	2.9	18	-	C
61	5	10.0	9.8	11	1	B
62	5	9.1	9.9	13	1	A
63	5	8.1	11.0	36	4	C
64	5	9.6	11.1	16	1	A
65	5,6	6.0, 14.4	12.3, 4.7	9, 8	1	B
66	5,6	6.8, 15.4	13.7, 6.5	15, 15	2	A
67	5	7.3	13.6	11	2	A
68	5	12.1	13.7	33	-	C
69	5	14.8	13.5	21	-	C
70	6	2.2	5.5	16	-	C
71	6	1.4	7.7	11	1	A
72	6	3.2	8.1	13	-	C
73	6	-0.5	11.3	92	-	C
74	6	2.3	12.3	37	3	B
75	6	10.8	8.3	65	4	A
76	6	8.2	10.5	16	2	A
77	6	14.0	7.6	12	-	C
78	6	14.9	8.1	13	-	C
79	6	14.1	9.7	9	-	C
80	6	11.8	11.0	12	1	A
81	6	13.0	8.5	8	1	B

APPENDIX B

CRATER CATALOG FOR MARS FROM MARINER 4 FRAMES 7 THROUGH 15

APPENDIX B

CRATER CATALOG FOR MARS FROM MARINER 4 FRAMES 7-15

Crater number	Frame(s)	Position (cm) from south	Position (cm) from west	Diameter (km)	Class	Quality
82	7	1.9	0.9	12	3	B
83	7	0.9	2.1	13	3	C
84	7	0.6	2.9	14	3	B
85	7	2.0	4.0	50	4	B
86	7	2.7	4.1	19	2	A
87	7	1.3	6.4	24	3	A
88	7	3.0	6.0	13	3	C
89	7	2.3	6.5	14	2	A
90	7	3.1	6.8	14	4	B
91	7,8	2.1, 11.2	10.2, 1.8	32, 30	3	A
92	7	2.3	11.5	27	4	C
93	7	4.8	2.4	8	2	C
94	7	5.8	3.2	10	2	A
95	7	3.7	5.9	66	4	B
96	7	5.1	5.2	7	2	B
98	7	6.6	6.4	8	2	B
99	7	6.0	8.0	14	3	B
100	7	6.0	11.4	31	4	A
101	7	6.3	12.7	9	2	B
102	7	12.2	3.0	10	1	A
103	7	11.5	2.8	14	3	B
104	7	10.7	3.3	11	3	C
105	7	9.8	3.4	11	3	B
106	7	9.7	1.4	12	3	B
107	7	9.6	5.1	10	3	B
108	7	8.8	6.6	7	3	B
109	7	10.8	6.4	21	3	A
110	7	9.9	8.9	38	4	A
111	7	13.9	6.9	11	4	A
112	7	11.0	11.1	9	1	A
113	7	9.9	12.0	26	2	A
114	7	10.3	12.8	10	2	A
115	7	12.2	10.9	5	2	B
116	7	9.2	13.5	7	2	A
117	7	10.7	14.3	5	2	B
118	7	12.0	15.1	9	2	B
119	7	15.5	9.7	19	1	A
120	7	14.3	11.9	14	4	A

APPENDIX B (Cont.)

Crater number	Frame(s)	Position (cm) from south	Position (cm) from west	Diameter (km)	Class	Quality
121	7	13.3	12.4	12	2	B
122	7	12.9	13.3	18	3	A
123	7	12.8	14.7	8	2	B
125	7	15.0	2.6	14	2	B
126	7	1.5	2.0	10	1	B
127	8	1.9	2.7	30	4	C
128	8	3.0	10.9	14	3	B
129	8	8.3	6.4	38	3	A
130	8	6.1	8.1	45	3	A
131	8	11.0	7.6	9	1	A
132	8	10.5	8.7	9	2	A
134	8	7.6	12.6	38	4	C
135	8	5.3	14.0	18	4	B
136	8	13.8	11.6	16	4	A
137	8	11.9	13.3	7	2	A
138	8	11.2	14.0	12	3	A
139	8	9.6	13.9	7	2	A
140	8	10.2	13.2	32	4	C
141	8	11.2	10.2	14	3	C
142	8	5.9	8.6	6	2	B
143	8	4.0	6.7	17	4	C
146	9	3.7	0.7	8	2	B
147	9	2.9	1.5	18	3	B
148	9	3.8	4.5	24	4	C
149	9	2.4	4.6	16	3	A
150	9	0.8	6.7	14	3	A
151	9	4.5	7.3	18	1	A
152	9,10	4.7,13.8	10.7, 3.2	12,9	3	B,C
153	9,10	3.4,12.8	10.6, 2.8	5,6	1	B,A
154	9,10	2.6,12.0	9.9, 2.1	11,10	1	A
156	9	5.8	2.4	9	2	B
157	9	7.3	2.5	12	3	B
158	9	9.6	2.1	13	3	A
159	9	7.2	4.5	19	4	A
160	9	7.1	5.5	18	2	A
161	9	9.1	5.4	27	3	A
162	9	10.2	6.2	9	3	C
163	9	9.8	6.6	6	1	A
164	9	8.0	6.1	7	2	B
165	9	6.4	8.0	7	2	B
166	9	8.1	8.0	33	4	A

APPENDIX B (Cont.)

Crater number	Frame(s)	Position (cm) from south	Position (cm) from west	Diameter (km)	Class	Quality
167	9	8.3	8.4	11	2	A
168	9	7.5	10.5	24	2	A
169	9	7.9	12.2	7	2	B
170	9	8.4	12.6	22	4	B
171	9	10.9	2.9	10	2	A
172	9	12.4	2.6	27	3	A
173	9	12.8	2.8	6	1	A
174	9	11.7	8.2	27	3	A
175	9	11.3	9.9	5	1	B
176	9	15.2	10.3	52	3	A
177	9	12.8	12.3	15	2	A
178	9	5.5	1.0	10	3	B
179	9,10	3.1,12.6	14.0, 6.1	17,25	4	C,B
180	9	4.8	9.5	30	4	C
181	9,10	5.2,14.4	11.5, 3.8	30,29	4	C,B
182	9	6.8	12.5	13	3	B
184	9	9.4	10.6	6	1	B
185	9	12.1	6.8	6	1	C
186	10	2.3	2.9	9	1	A
187	10	4.5	5.7	33	3	A
188	10	2.5	10.5	34	4	B
189	10	-2.0	8.0	121	3	A
190	10	6.1	3.2	6	1	A
191	10	8.0	3.3	25	4	A
192	10	9.7	4.0	36	4	B
193	10	9.3	5.2	26	4	B
194	10	8.8	6.1	11	2	A
195	10	9.6	7.1	24	4	B
196	10	8.0	8.6	43	4	C
197	10	6.9	8.7	10	2	A
198	10	7.6	11.4	38	3	A
199	10	7.3	12.7	7	1	A
200	10	5.8	16.5	112	3	A
201	10	8.5	14.3	9	2	A
202	10	11.0	8.8	37	4	C
203	10	10.2	10.4	37	4	C
204	10	12.4	9.6	27	3	A
205	10	14.7	6.5	9	1	A
206	10	13.3	11.2	19	4	A
207	10	13.2	12.6	8	4	C
208	10	3.9	10.1	13	3	C
209	10	7.1	4.6	22	3	A
210	10	6.6	4.0	22	3	B

Crater number	Frame(s)	Position (cm) from south	Position (cm) from west	Diameter (km)	Class	Quality
211	10	14.1	7.6	21	4	B
212	11	4.1	1.3	7	2	A
213	11	7.0	3.4	31	1	A
214	11	5.6	5.3	16	1	A
215	11	3.4	12.5	24	4	A
216	11	2.0	12.4	19	4	B
217	11	7.4	6.2	149	3	A
218	11	10.0	3.9	33	4	C
219	11	11.2	4.2	5	1	B
221	11	9.2	11.1	7	1	A
222	11	8.5	11.4	6	2	A
223	11	9.5	12.1	16	3	A
224	11	12.0	13.8	68	2	A
225	11	13.6	1.1	20	1	A
226	11	14.5	1.7	13	3	B
227	11	14.4	3.2	11	4	A
228	11	13.0	4.9	32	2	A
229	11	12.6	8.2	7	1	A
230	11	13.7	9.8	5	2	C
231	11	13.7	10.7	21	3	B
232	11	13.9	12.1	10	1	A
233	11	-1.2	11.9	64	3	C
234	11	4.1	6.3	17	4	C
235	11	2.5	6.5	32	4	B
236	11	1.9	5.7	18	3	C
237	11	3.9	4.6	39	4	B
238	11	8.0	4.5	15	4	C
239	11	14.9	2.7	12	4	C
240	11	7.1	12.6	22	4	C
241	11	8.7	13.7	24	4	C
242	11	5.2	1.4	6	2	B
243	11	4.6	1.4	5	2	B
244	12	2.7	0.0	65	4	B
245	12	7.4	2.0	12	2	A
246	12	8.4	3.1	6	2	A
247	12	7.3	5.4	8	1	A
248	12	8.9	7.7	11	2	A
249	12	3.6	13.9	13	1	B
250	12	4.1	14.7	18	2	C
251	12	6.9	13.7	19	2	B
253	12	12.8	13.8	31	3	A
254	12	12.8	9.9	41	4	B
255	12	13.1	2.7	31	4	C

Crater number	Frame(s)	Position (cm) from south	Position (cm) from west	Diameter (km)	Class	Quality
257	13	12.4	0.6	13	3	A
258	13	13.7	2.7	13	4	B
259	13	12.0	4.0	19	4	C
260	13	13.0	7.6	37	4	A
261	13	11.9	9.7	28	3	A
262	13	11.6	9.3	15	2	A
263	13	13.0	11.1	11	3	A
264	13	15.0	11.7	9	4	A
265	13	7.0	8.0	11	4	B
266	13,14	6.0,15.0	11.5, 4.1	40,42	4	A
267	13	7.2	14.0	10	3	A
268	13,14	3.9,12.5	12.5, 5.1	7,5	2	A
269	13,14	2.3,10.7	12.4, 5.1	41,45	3	A
270	13	13.8	11.3	11	3	C
271	13	14.0	5.9	9	2	B
272	13	10.3	9.3	23	4	C
273	13	5.6	12.6	14	3	B
274	13	6.7	5.2	21	4	C
275	13	5.1	6.6	20	4	C
276	13	3.9	8.0	36	4	C
277	14	4.4	6.5	21	4	A
278	14	3.3	10.2	33	4	A
279	14	1.4	11.7	12	4	B
280	14	6.9	6.2	18	4	A
281	14	11.4	9.2	7	1	A
282	14	8.4	10.2	86	4	A
283	14	9.8	12.4	12	4	B
284	14	10.9	14.4	41	2	A
285	14	14.6	11.3	22	4	C
286	14	12.5	12.2	43	4	B
287	14	6.9	11.4	19	4	C
288	14	7.4	9.6	19	4	C
289	14	8.4	9.0	22	4	C
290	14	4.4	4.6	58	4	C
291	14	2.5	6.0	8	1	A
292	14	1.8	6.8	9	1	A
294	15	1.4	12.5	22	2	C
295	15	7.8	8.1	19	4	C
296	15	11.8	6.0	26	4	A
297	15	13.0	7.3	18	4	B
298	15	14.5	10.2	37	4	A

BIOGRAPHICAL NOTES

CLARK R. CHAPMAN currently holds a graduate assistantship in the Department of Meteorology at the Massachusetts Institute of Technology. He did undergraduate study in astronomy at Harvard College and received his B. A. in 1967. Mr. Chapman has worked at the Lunar and Planetary Laboratory of the University of Arizona, the Department of Geology and Geophysics of M. I. T., and the Smithsonian Astrophysical Observatory.

JAMES B. POLLACK received the A. B. degree from Princeton in 1960, the M. A. degree from the University of California at Berkeley in 1962, and the Ph. D. degree from Harvard University in 1965.

Dr. Pollack currently holds an appointment as physicist on the staff of the Smithsonian Astrophysical Observatory. His research specialties include theoretical studies of planetary atmospheres, cloud layers, and surfaces.

CARL SAGAN received the A. B., S. B., S. M., and Ph. D. degrees from the University of Chicago in 1954, 1955, 1956, and 1960, respectively.

Since 1962 he has held joint appointments on the staffs of Harvard College Observatory and the Smithsonian Astrophysical Observatory. He is also a consultant to the National Aeronautics and Space Administration and the National Academy of Sciences.

Dr. Sagan's investigations include studies of the physics and chemistry of planetary atmospheres and surfaces, exobiology, and the origins of life.